Master of Science Thesis

MRI only radiotherapy using synthetic CT images

Dosimetric accuracy and patient positioning strategies in an MRI only workflow

---

Emilia Persson

Department of Medical Radiation Physics
Clinical Science, Lund
Lund University, 2015

Supervisors:
Fredrik Nordström, Carl Siversson and Crister Ceberg

Abstract

Background and purpose: Magnetic resonance imaging (MRI) only radiotherapy has, due to superior soft tissue contrast of MRI and the possible reduction of systematic uncertainties, grown into a promising technique. The purpose of this work is to investigate parts of an MRI only workflow with synthetic computed tomography (sCT) images generated from MRI. This was done through investigation of treatment planning abilities and patient positioning strategies in a suggested MRI only workflow for prostate cancer patients.

Material and methods: A novel atlas based generation method, The Statistical Decomposition Algorithm (SDA), was used for sCT generation. sCT images of six patients were evaluated visually and using the DICE similarity index. Treatment plans (Intensity modulated radiation therapy (IMRT) and protons) were calculated based on conventional CT and sCT and compared using clinical dose-volume histogram (DVH) criteria and gamma evaluation. Patient positioning in the MRI only workflow were investigated through two studies, including five patients. The ability to identify implanted gold fiducials in MRI was investigated and a MV bone match procedure tested with digitally reconstructed radiographs (DRR).

Results: The image analysis implicated minor problems with the bone surfaces in the generated sCT, and some disparities compared to CT were noted. The treatment planning study showed that treatment planning on sCT introduced a mean dose difference to PTV of -0.2% to -0.1% compared to CT. Gamma analysis showed a mean pass rate close to 100% for IMRT (1%/2mm) and 93% for protons (3%/2mm). The fiducial marker identification study showed that the fiducials could be identified, in all cases but one. In this case a marker was identified centimeters from the right position. The bone match showed differences of 0.7-0.9 mm between match performed with CT-DRRs and sCT-DRRs images towards MV images.

Conclusion: Good agreement in terms of dose accuracy was found when dose distributions were compared between sCT and CT treatment plans. The image evaluation indicated disparities in the bone surface between sCT and CT, but this had only small effect on the resulting dose distributions for photon plans. Patient positioning strategies needs further work and guidelines have to be developed. The initial results of this study show a problem with transferring the fiducial marker positioning strategies in the conventional workflow to the MRI only workflow. The MV bone match can be performed and, although it may not be the preferred procedure for prostate patient, the study showed good results and can be usable for other diagnosis.

Popular scientific summary in Swedish

Sedan sent 1800-tal har strålterapi använts för behandling av cancer. 50% av alla cancerpatienter blir någon gång behandlade med strålterapi, som är en avancerad teknik med många olika steg för att uppnå den slutgiltiga behandlingsplanen. Patienten börjar sin strålbehandlingsresa med att bli diagnosticerad och får sin behandling ordinerad. Efter detta startar förberedelserna inför strålbehandlingen, vilket är en lång process innan behandlingen kan ges. För att kunna skapa den behandling som är ordinerad måste man först ha bilder på patienten där cancern och organ syns. Dessa bilder används för att bestämma vart strålningen skall riktas och vilka områden som önskas undvikas. Detta görs för att uppnå bästa möjliga behandlingsresultat, samtidigt som biverkningar undviks.

De bilder man använder till strålbehandlingen fås från en så kallad skiktröntgen. Denna ger tredimensionella bilder av patienten där man önskar kunna se cancern samt omkringliggande organ. Denna bild skickas till det som kallas för dosplaneringssystemet, vilket är det system där behandlingen skapas. Man beräknar här hur mycket strålning som skall ges till cancern, samt justerar så att strålningen till omgivande organ inte blir över rekommenderade gränser. Att kunna utföra detta kräver att cancern är väl utritad på skiktröntgenbilderna, vilket kräver att man kan se skillnader mellan mjukdelarna i kroppen. Tyvärr är en av de stora nackdelarna hos skiktröntgen att det är svårt att skilja mellan olika mjukdelar i bilderna. Detta leder till att cancern och organen i patienten kan vara svåra att hitta exakt, vilket i sin tur leder till att man riskerar att inte kunna ge den önskade behandlingen.

För att lösa problemet med de bristfälliga bilderna har forskare riktat in sig mot användningen av en annan bildgivande teknik – magnetkameran. Magnetresonans (MR) är en bildgivande teknik som ger tredimensionella bilder av patienten utan att använda röntgenstrålning. MR använder starka magnetfält för att påverka vattnet i kroppen, vilket ger bilder med mycket god skillnad mellan mjukdelarna i kroppen. Dessa bilder är i många fall idealiska för bestämning av cancerns position, vilket i sin tur kan leda till bättre behandlingar.

De system som idag används för att skapa behandlingarna är utvecklade för att passa bilder från skiktröntgen och problematik uppstår när bilderna från magnetkameran ska användas. Bilderna från magnetkameran passar inte för att utföra de beräkningar av stråldoserna som behövs inför behandlingen. För att lösa detta problem har forskare föreslagit att man omvandlar de bilder som kommer från magnetkameran till bilder som liknar skiktröntgenbilderna. Man kan på så vis hitta cancern och organen på MR bilden, sedan omvandla bilden för att kunna beräkna stråldoserna.

Precis som alla nya tekniker så medför införandet av ny teknik mycket tester innan slutprodukten kan utnyttjas. Detta gäller även för införandet av ny teknik i strålbehandling. Detta arbete föreslår och utvärderar en ny strålbehandlingsmetod med MR bilder och jämför denna med den gamla metoden med skiktröntgenbilder. Önskvärt var att se om den nya tekniken gav likvärdiga resultat som de gamla och utvärdera dess användbarhet. Undersökningar visade att den nya tekniken med MR gav mycket lovande resultat och kan potentiellt eliminera osäkerheter som den gamla metoden bidrar med. En ny bildteknik utan strålning kan erbjuda många fördelar jämfört med den gamla tekniken, både i diagnostiskt syfte och ur behandlingssynpunkt. Vidare undersökningar av metoden förväntas leda till införandet av en ny metod för strålbehandling, anpassad till de nuvarande krav som ställs på cancerbehandlingar.

Abbreviations

PTV	Planning Target Volume
OAR	Organs at risk
CT	Computed Tomography
MRI	Magnetic Resonance Imaging
HUs	Hounsfield Units
sCT	Synthetic Computed Tomography
SDA	The Statistical Decomposition Algorithm
DTA	Distance To Agreement
rCT	Deformable Registered Computed Tomography
IMRT	Intensity Modulated Radiation Therapy
CTV	Clinical Target Volume
AAA	Anisotropic Analytical Algorithm
PBA	Pencil Beam Algorithm
DVH	Dose Volume Histogram
TPS	Treatment Planning System
DRR	Digitally Reconstructed Radiograph
CBCT	Cone Beam Computed Tomography

Table of contents

1. Introduction

1.1 Background

Radiation therapy has been used since late 19th century and has since then developed into a technique with great variability, enabling care for many malignant diseases. About 50% of the patients diagnosed with cancer are at some point treated with radiation therapy, where the technique stands for 30% of the cure of cancer patients worldwide (Cancerfonden, 2015). The main goal is to treat or control the cancer, which in external radiation therapy is done by aiming high energy radiation to an area located inside the body called the planning target volume (PTV). In combination with delivering a high absorbed dose to the PTV, organs at risk (OAR) and normal tissue should be avoided in order to minimize side effects. To accomplish this, high accuracy is needed in all steps of the treatment process, often referred to as the radiotherapy chain or the radiotherapy workflow.

The radiotherapy chain includes all steps from treatment prescription to completed treatment. The CT is today the gold standard imaging modality in radiotherapy, and the CT images are used throughout the entire radiotherapy chain. The treatment planning system (TPS) requires Hounsfield units (HUs) for absorbed dose calculations, which in a conventional workflow is received directly from the CT. However, for some diagnoses, such as prostate cancers, a set of magnetic resonance imaging (MRI) is preferable for more precise target delineation (Parker et al., 2003). Through co-registration of the MRI and CT, using implanted fiducial markers in the prostate, the both modalities can be used for target delineation while the CT constitutes the base for treatment planning. When the final treatment plan is approved and clinically tested and verified, the patient can begin the treatment. The treatment procedure includes several steps, such as positioning, imaging and finally delivery of the prescribed treatment. After this, follow up can be done in order to see if and how the tumor has responded to the treatment.

Although the co-registration of MRI and CT for prostate patients is common, the geometric accuracy of the method has been questioned (Korsholm et al., 2014). The MRI and CT are unlikely to be geometrically comparable, and the co-registration process is therefore associated with uncertainties (Lambert et al., 2011). With the ambitions to improve the workflow and minimize the geometrical and dosimetrical uncertainties, researchers have been focusing towards the use of solely MRI in combination with radiotherapy - called MRI only radiotherapy (Johansson et al., 2011, Siversson et al., 2015, Korhonen et al., 2014, Dowling et al., 2012, Andreasen et al., 2015).

The increased interest of an MRI only workflow in radiotherapy has emerged due to the superior soft tissue contrast that MRI provides. It has been shown that an MRI only workflow can reduce the systematic uncertainties from 3-4 mm to 2-3 mm when compared to a combined CT/MRI workflow for prostate patients (Nyholm et al., 2009). The main contributing factor of the reduced uncertainties was exclusion of the co-registration process needed in a combined CT/MRI workflow. Less inter-observer differences have also been shown for prostate patients when delineating the target on an MRI (Parker et al., 2003) which is a result of the improved soft tissue contrast. The improvement of the soft tissue contrast also results in a reduced irradiated rectum volume, since the target volume estimated on MRI in general is smaller than on a CT (Debois et al., 1999). The exclusion of the CT in the radiotherapy workflow for prostate patients would not only reduce the geometrical uncertainties, but also provide reduced costs as the CT can be excluded. This, in combination with the possibility of a non-ionizing imaging method, makes the MRI only workflow an alternative that deserves further considerations.

In an MRI only workflow, the CT would be replaced with an MRI in every step of the chain. Since the MRI data doesn't directly translate into HUs, a conversion is required. In order to accomplish this, the concept of a synthetic CT (sCT) has emerged. A synthetic CT image is a substitute for the CT, generated from MRIs through various methods. The idea of an MRI radiotherapy workflow has interested several groups of researchers, and encouraged them to develop different types of sCT generation methods. Some groups suggest generation methods where individual voxels are classified into tissue types (Johansson et al., 2011). Other groups have investigated a method where the sCT generation relies upon a database of several tissue types, originated from multi template patient materials (Siversson et al., 2015). Regardless of the sCT generation method, the aim is to produce a substitute CT image from an MRI and thus enabling an MRI only workflow.

From selection of generation method to positioning strategy, there are various ways to go and several options to choose from. Regardless of the choice of strategy, the reliability of the sCT is essential, as both treatment planning and patient positioning is dependent on the result.

1.2 Aim

This thesis focuses on parts of an MRI only radiotherapy chain where synthetic CT images can replace the gold standard CT in the workflow for prostate cancer patients.

The aims were investigated with an MRI only workflow as foundation – and compared to a combined CT/MR workflow. The following specific aims were formed for this thesis:

- Investigate the image similarities of sCT and CT images and detect where, if any, dissimilarities can be found.
- Create treatment plans of various natures and compare absorbed dose calculation results between sCT and CT.
- Investigate patient positioning strategies in an MRI only workflow.

Advantages, challenges and future perspectives with a potential MRI only workflow will be discussed.

2. Theory

2.1 sCT generation methods

2.1.1 General

The generation methods can be divided into two major groups – Voxel based and atlas based generation methods. However, some methods are a combination of the two major groups.

Johansson et al. has developed a voxel based generation method that uses a trained set of matched MR and CT data to predict a sCT. They uses a Gaussian mixture regression model that makes use of three different MR sequences, a T2 weighted spin echo and two dual echo ultra short echo time sequences. The model links the voxel values in images from the MR sequences to the CT voxel values (Johansson et al., 2011). Dowling et al. have instead of the voxel approach chosen an atlas based generation method, developed for prostate patients. In order to generate a sCT they make use of a multi-modality atlas of registered MRIs and CTs, and register the MRIs to the patients MRI scan. The MRI sequences in this work was two T2 weighted scans and one T2* scan. Through transformation and deformations of the corresponding CT atlas, a sCT can be created according to the patient anatomy (Dowling et al., 2012). In the current article, the sCT is referred to as a pseudo CT (pCT), which is a common name for the generated CT substitute.

The atlas and voxel based methods have different advantages, but are also associated with drawbacks. The voxel based methods have the drawback that exotic pulse sequences often is required for discrimination between bone and air (Jonsson et al., 2013), while the atlas based methods relies upon a direct database which can be troublesome for patients with atypical anatomy (Dowling et al., 2012).

Korhonen et al. suggests in their work a dual model HU conversion method. The method converts MRI intensity values into HUs for prostate cancer patients. The pCT is created from a combination of T1/T2* sequences and CT data (Korhonen et al., 2014). This technique differs from the atlas and voxel based methods in the way that they do not directly make use of the voxel values or of an atlas database. This is also the case for Andreasen et al. which technique creates pCTs from T1-weighted scans using a database of patches. The patch is defined as a cube with *m* voxel size side length in an MRI (Andreasen et al., 2015). This technique is in some manor an atlas based method, but with a unique procedure that replaces the patient atlas with patches.

The sCT images investigated in this thesis were generated using the Statistical Decomposition Algorithm (SDA), which is a novel method for generating sCT images from MRI-based material. The SDA is presented in a parallel work accepted for publication (Siversson et al., 2015). The method is soon to be released as a clinical product developed by Spectronic Medical AB in collaboration with researchers from Lund University. This product will also be used in the Swedish project Gentle Radiotherapy, which is an effort to incorporate MRI in the radiotherapy chain.

2.1.2 The Statistical Decomposition Algorithm

The automated SDA method is an atlas- based method that makes use of a multi-template assisted classification method. The MRI is automatically decomposed into several tissue types, whereupon the tissue types are statistically analyzed. The statistical analysis finds the most probable CT representation for the particular individual, depending on several features such as shape- and textures of the tissue types. The SDA uses a multi template material, consisting of both MRI and CT from various patients, to create the most likely CT representation for each tissue type. Finally, the sCT is generated through fusion of the individual tissue types. Figure 2.1 illustrates the SDA method in a simplified manner from the point of incoming MRI patient material, to final representation of the sCT.

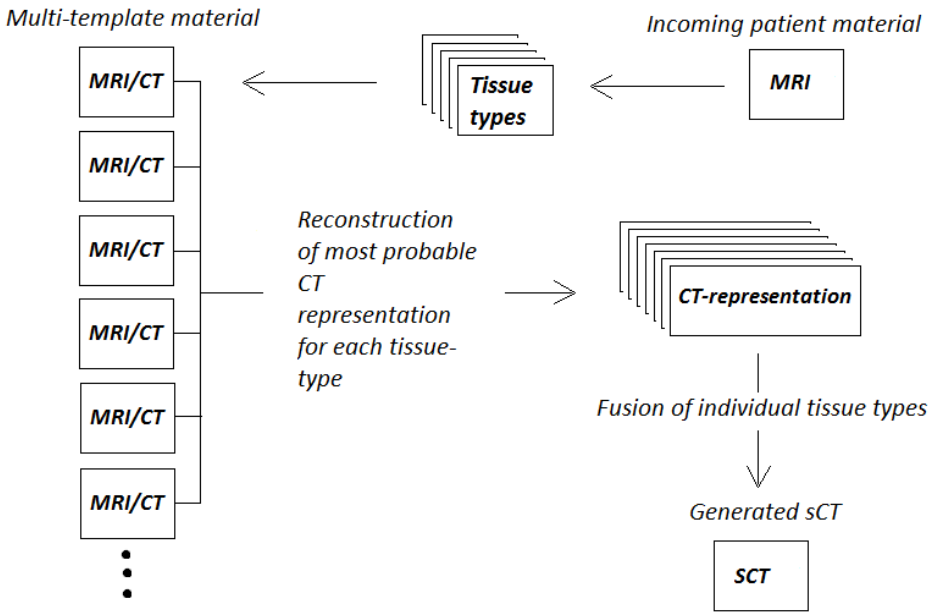

Figure 2.1 The SDA method illustrated from starting point to final generation of the sCT. The incoming MRI patient material is decomposed into tissue-types and compared to the multi-template material consisting of several patients. The most probable CT representation is found in the atlas for each tissue-type and the sCT is generated through fusion of the individual tissue-types.

2.2 The DICE similarity index

The original version of the DICE similarity index (Dice, 1945) was initially developed for the field of ecology. At the time there was no good measure to express how two different species were associated in nature, and so the DICE similarity index was presented. The article suggests an equation where the resulting index ranges from 0 to 1, where 0 indicates no association and 1 shows complete association of the two species examined in all samples. Although the original paper was directed to the field of ecology, the DICE similarity index is also a common method in the field of image processing. In recent works, the index is used for evaluation of generated sCT images (Jonsson et al., 2015, Andreasen et al., 2015). The DICE similarity index will in this work be used according to the following equation:

$$D = \frac{2 \cdot O}{a+b} \cdot 100 \tag{2.1}$$

Where O is the number of pixels that agrees in the images A and B, called overlapping pixels, and variables a and b corresponds to the number of pixels in image A and B respectively. If image A and B are identical, the number of pixels in each of the images is the same. This leads to that if the number of pixels that are overlapping in the two images are multiplied with two, this should correspond to the summation of a and b. If there is any dissimilarity, this leads to a smaller number of overlapping pixels, than expected when the pictures totally agree. Finally, in order to get a measure of the similarity of the images, the multiplication of the overlapping pixels are divided with the summation of a and b. This multiplied with 100, gives the measure in percent of pixels that agrees in the images. This is what is referred to as the DICE similarity index, D, demonstrated with two examples in Figure 2.2.

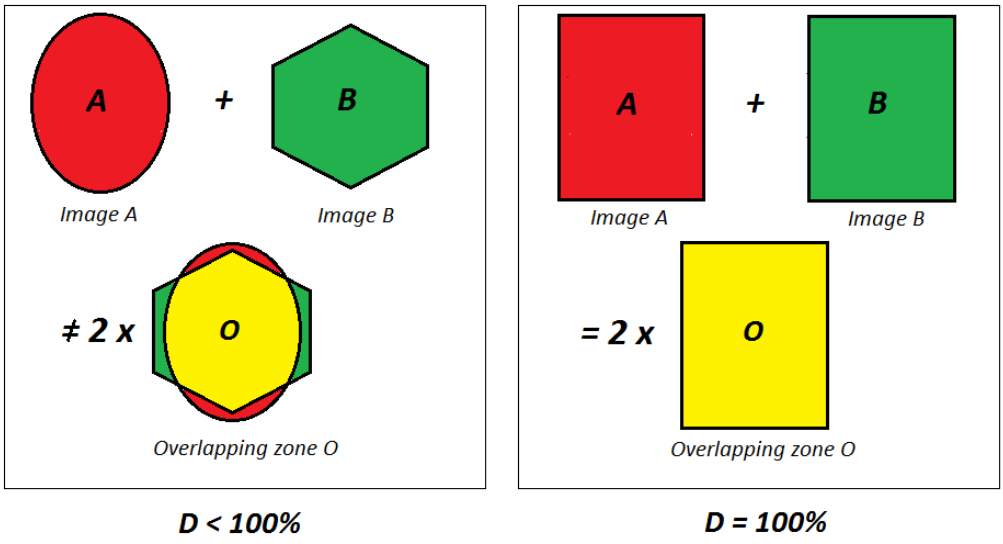

Figure 2.2 The figure demonstrates the idea behind the DICE index used in this work. If A and B are compared to each other, differences can be detected if present. If A and B were identical, the sum of the pixels in A and B should correspond to the number of pixels in O multiplied by 2. To the left we can see examples were the DICE similarity index would not be equal to 100%, due to dissimilarities in A and B. The summation of pixels in A and B will be larger than twice the number of the pixels in O, leading to D<100%. To the right we have an example were A and B exactly agrees, which leads to D=100%.

2.3 Gamma evaluation

The gamma evaluation method is used for comparison of dose distributions and was proposed by Low et al, 1998 for comparison of two-dimensional dose distributions. Low presented a method for comparison between measured and calculated dose distributions by the use of dose differences and distance to agreements (DTA). In the original version, the comparison is made between a measured point, $\boldsymbol{r}_m$, and a calculated point, $\boldsymbol{r}_c$, in the two compared dose distributions. In this thesis, these will be replaced with points in two calculated dose matrices, one reference point, $\boldsymbol{r}_r$, in the reference dose distribution and one evaluated point, $\boldsymbol{r}_e$, in the evaluated dose distribution. Low uses the measured dose distribution as a reference and the calculated as evaluated distribution, hence $\boldsymbol{r}_r$ replaces $\boldsymbol{r}_m$ and $\boldsymbol{r}_e$ replaces $\boldsymbol{r}_c$.

The method uses acceptance criteria, the dose difference criterion ΔD_R, and the DTA criterion Δd_R. These two criteria can be visualized as an ellipsoid where the surface represents the acceptance criteria; this is illustrated in Figure 2.3. The equation of the ellipsoid is

$$1 = \sqrt{\frac{r^2(\boldsymbol{r}_r,\boldsymbol{r})}{{\Delta d_R}^2} + \frac{\delta^2(\boldsymbol{r}_r,\boldsymbol{r})}{{\Delta D_R}^2}} \tag{2.2}$$

The right hand side of equation 2.1 can be used to define the gamma index. The gamma index is defined as:

$$\gamma(\boldsymbol{r}_r) = min\{\Gamma(\boldsymbol{r}_r,\boldsymbol{r}_e)\}\ \forall(\boldsymbol{r}_e) \tag{2.3}$$

Where

$$\Gamma(\boldsymbol{r}_r,\boldsymbol{r}_e) = \sqrt{\frac{r^2(\boldsymbol{r}_r,\boldsymbol{r}_e)}{{\Delta d_R}^2} + \frac{\delta^2(\boldsymbol{r}_r,\boldsymbol{r}_e)}{{\Delta D_R}^2}} \tag{2.4}$$

The spatial difference between the reference and the evaluated point is represented by $r(\boldsymbol{r}_r,\boldsymbol{r}_e)$ and $\delta(\boldsymbol{r}_r,\boldsymbol{r}_e)$ represents the absorbed dose differences between the reference and evaluated point. The gamma calculation is made for a single point in the reference distribution against all reference points.

If any point in the evaluated matrix meets the selected criterion the reference point passes, and the evaluated point can be seen as located inside of the ellipse. If none of the evaluated points fulfill the chosen criterion, the reference point fails. The pass-fail criteria are defined as:

$$\gamma(\boldsymbol{r}_r) \leq 1 \text{ Point passes} \tag{2.5}$$

$$\gamma(\boldsymbol{r}_r) > 1 \text{ Point fails} \tag{2.6}$$

If several reference points are evaluated, the gamma pass rate can be defined as the ratio between the number of points that passes the gamma calculation and the total number of points evaluated. The gamma evaluation is applicable in 1-3 spatial dimensions.

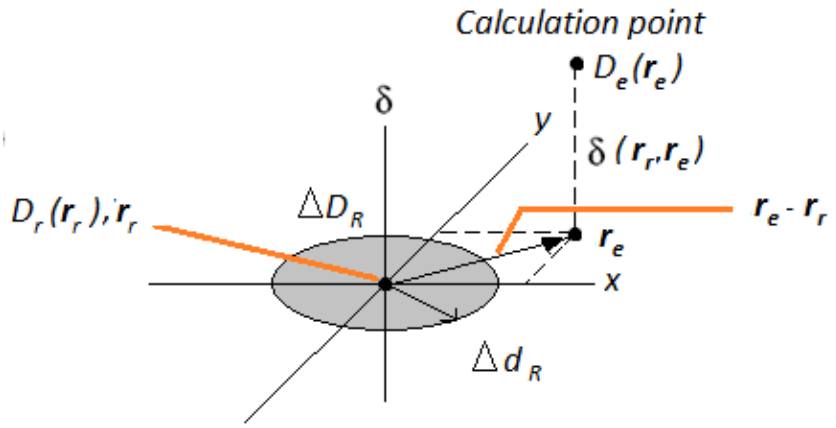

Figure 2.3 A geometrical representation of the gamma evaluation method for a 2D dose distribution, with combined criterions for dose differences and DTA. The figure is drawn based on the figure in the original paper on the gamma evaluation method (Low et al., 1998). The x- and y-axes represents the spatial plane and the δ axis represents the dose differences between the measured and calculated absorbed doses.

3. Material and Methods

3.1 The MRI only workflow

As a foundation for this thesis, an MRI only workflow using sCT was suggested. The workflow covers the steps from the point where the patients are positioned prior to imaging in the treatment fixation, to follow up after completed treatment. The MRI only workflow was designed with the conventional workflow for prostate cancer patients in mind and within every step where a CT is used an MRI or sCT was inserted. The main parts were the sCT takes part is in the target and risk organ delineation, generation of the sCT and the following treatment planning. After this the plan is verified and tested, according to the routines at the particular treatment clinic, and finally the patients are ready for positioning prior to treatment. The positioning includes several steps, and depending on the technique available, the positioning procedure can differ. In the suggested workflow, the positioning was divided into soft tissue and bone or fiducial markers. Positioning with fiducial markers is a well-established strategy for prostate patients. When this is not possible, a bone and soft tissue match can be performed. The use of solely soft tissue match would preferably be performed with an MRI combination were the patients can be positioned according to a nearby MRI (Karlsson et al., 2009) or with the use of an integrated MRI Linear accelerator (Lagendijk et al., 2014). After positioning the patients can be treated according to prescription and after completed treatment, follow up can be achieved if required. With MRI, the possibility of follow up during and after treatment is enabled without excess radiation.

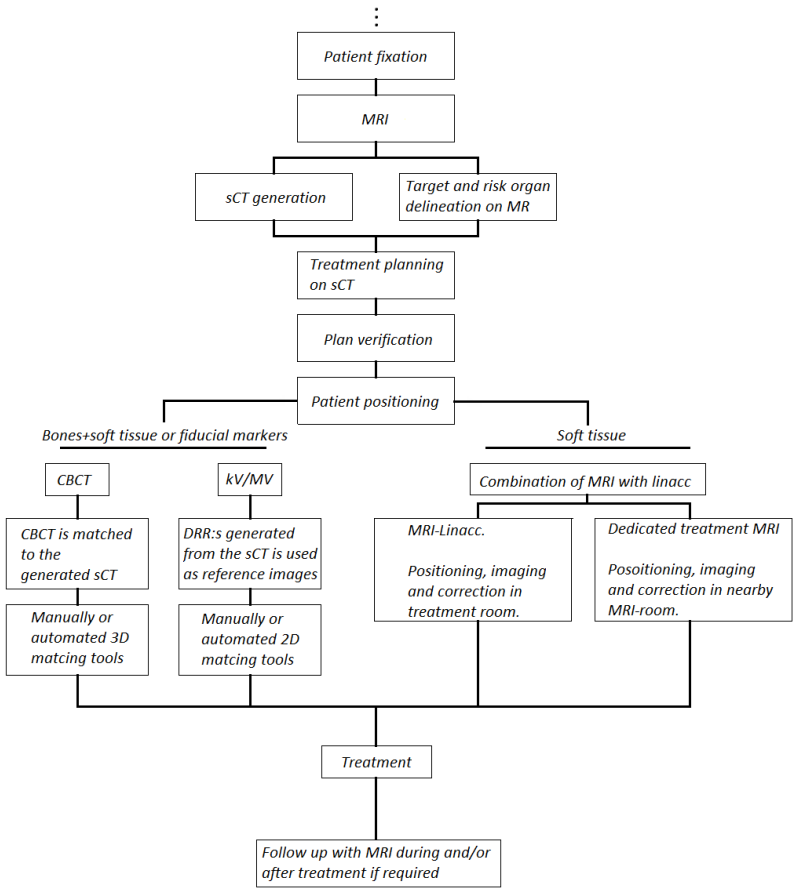

Figure 3.1 Suggested MRI only workflow. In this work the CBCT was referred to as a bone and soft tissue matching procedure. The bones were considered as the matching object in CBCT and the soft tissue as a guide to the match. Rectum and bladder should have the same degree of filling as when the treatment planning images was acquired, in order to deliver the treatment as planned. A solely soft tissue match would preferably require soft tissue visualization, which could be done with an MRI according to the right hand side of the workflow. The CBCT and kV/MV match could be used as a solely bone match procedure.

3.2 Patient material

Datasets with images of 11 patients, treated for prostate cancer, were received from Umeå University and included in this study. The patients' primary diagnosis was not considered when target and risk organs were delineated, but instead each patient was considered as having strictly the prostate as the CTV.

Six of the patients were included in the image analysis and the treatment planning study and the remaining five patients were included in the positioning study. The division into two groups was necessary, since all patients didn't have the image material needed for both studies. The time limit of the thesis, and limited patient material, restricted the use of larger patient selections for each study.

3.3 Image material

Prior to treatment prescription, each patient included in the study had an MR and a CT image session. The MRI was acquired with an Espree 1,5T scanner (Siemens Healthcare, Erlangen, Germany), using a T2 weighted 3D turbo inversion recovery sequence (SPACE). This was acquired with repetition time 1500 ms, echo time 208 ms and a flip angle of 150°. The image matrix was $384\times384\times120$ voxels with the voxel size $1{,}1\times1{,}1\times1{,}7$ mm, and the field of view was set to surround the outer body contour for each individual patient case. The CT images was acquired using a SOMATOM Emotion 6 scanner (Siemens Healthcare, Erlangen, Germany), with in plane resolution ranging from 0.86 to 0.96 mm with slice thickness 2.5 mm.

The patients were positioned with the same strategy prior to both MR and CT, with fixation of the feet and with knee support. The MR images were acquired directly after the CT, in order to minimize the effect of organ movements and deformations (e.g. filling of the rectum and bladder) between imaging sessions. The patients had no food restrictions prior the imaging sessions. The rectum diameter was controlled on the CT overview image and the imaging proceeded if a rectum diameter of less than four centimeter was measured. If not, the patient was asked to visit the toilet before the imaging proceeded.

The MRI was used for generation of the sCT according to the SDA based method developed by Spectronic Medical AB, who also provided the sCT images. The resulting sCT images were of the same resolution and had the same frame of reference as the MRI. In order to evaluate the sCT, without introducing errors originating from repositioning between MRI and CT, an additional set of CT images was generated, called registered CT (rCT). The concept of an rCT image comparison have been suggested in a parallel work accepted for publication (Siversson et al., 2015). The rCT images were created by Spectronic Medical AB, using deformable registration and the elastic toolbox, in which each CT was registered to its corresponding MRI. This enables the sCT to be compared to the CT without including the errors introduced by the repositioning and excludes the effect of geometrical distortions. The rCT can be compared to the CT in order to evaluate the errors introduced by the multiple imaging sessions required in a combined workflow.

The patient positioning study required images from the patient positioning sessions obtained during treatment. The available images from the treatment sessions at Umeå were orthogonal MV images, which were received along with MR, CT and MR images for fiducial marker identification.

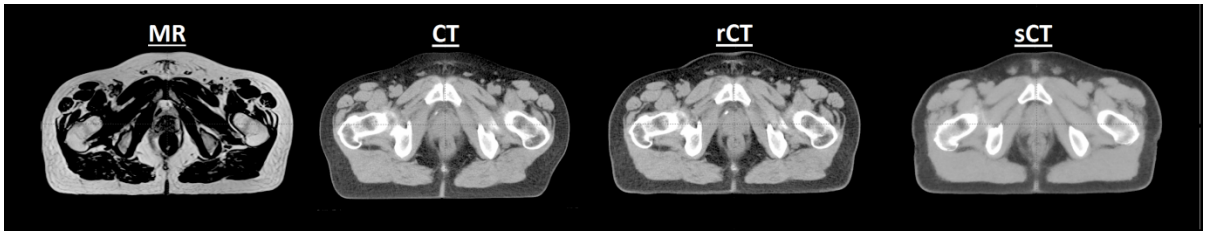

Figure 3.2 Images received from Umeå university hospital, MRI and CT, and from Spectronic Medical AB, rCT and sCT. The images displayed belong to patient case 1, and the other patient cases contained the same image information.

3.4 Image evaluation

The hypothesis was that differences were expected to be found in the bones in the images, particularly at the bone surfaces. This is expected since the sCT is created from an MRI were no bones can be seen. For this reason it was the bony structures that were chosen as a measure of the agreement of the images. The higher attenuation in bones, compared to muscle and fat, can result in a larger error in dose distribution if the bones are positioned differently.

The images were evaluated with the DICE similarity index. The evaluation gives a measure of the agreement (i.e. similarity) between the generated sCT and the original CT. For the comparison, the rCT worked as reference and was compared to the sCT and the CT. MATLAB (The MathWorks inc.) was used for the evaluation. A threshold of 200 HU was set to identify and segment the bones in the images, whereas those pixels identified as bones were set to 1 and otherwise 0. The pixels were summarized in each of the three image matrices and the number of overlapping pixels in sCT/rCT and CT/rCT was calculated. Finally equation 2.1 was used for calculation of the DICE similarity index. The DICE similarity index was expressed in percent, where 100% corresponded to a perfect agreement between the binary images. An index below 100% pictured a difference. Since the index merely gave a number of the agreement between the images, further analysis was needed to detect where the potential differences appear. The threshold images were overlaid in MATLAB and the differences were colored in order to visualize the in dissimilarities.

In order to make a fair comparison, concentrated to the bone surface, the cavities arising from the threshold were filled prior to the DICE calculation. The DICE index was calculated in 20 slices surrounding the PTV and the mean DICE value were calculated for each patient. This was done in order to minimize the effect of the threshold and slice selection.

3.5 Treatment planning

Cancer treatment with external radiation therapy is a technique that has a large variety of modalities available. RapidArc and IMRT are modalities commonly used for treatment of prostate cancer, and IMRT was one of the modalities chosen for evaluation in this work. RapidArc had already been showing promising results in a parallel work (Siversson et al., 2015), and is for this reason excluded from this work. The use of other modalities than RapidArc was done to test the usability of the sCT concept with different treatment techniques, in order to evaluate the MRI only chain with a wider perspective. Different techniques may be differently sensitive to insecurities in HUs, and therefore IMRT was investigated. The hypothesis was that IMRT could be more sensitive to density differences than RapidArc. A difference in density along the path of the radiation fields should have a greater influence on the dose distribution from IMRT compared to RapidArc. RapidArc radiates in all angles around the patient, and the density effect should therefore be of less impact for this technique.

Proton therapy is another modality that can be used for treatment of prostate cancer. The Scandinavian Proton Therapy Center Skandionkliniken is scheduled to open for treatments in summer 2015. Based

on the increased availability of proton treatment, both nationally and internationally, this modality was also included in the evaluation of sCT for treatment planning.

3.5.1 IMRT treatment planning

Two five field sliding-window IMRT treatment plans, with energies 6MV and 10 MV respectively, was generated for each patient using the Eclipse treatment planning system (Varian Medical systems, Palo Alto, CA). The prostate and OARs were automatically segmented using the MriPlanner software (Spectronic Medical AB, Sweden) on the MRI, according to the idea of an MRI only workflow. The structures were copied and transferred to the image sets used. The PTV was created through expansion of the clinical target volume (CTV) with 7 mm in all directions.

The prescribed dose was 78 Gy with 2 Gy per fraction. All treatment plans was created with the gantry positioned at 40, 110, 180, 250 and 320 degrees. The plans were optimized using the Dose volume optimizer, version 10.0.28, and a final dose calculation was made with the anisotropic analytical algorithm (AAA) version 10.0.28. All plans fulfilled the dose volume constraints of the conventional arm of the Swedish multicenter Phase III study of HYPO-fractionated Radiotherapy of intermediate risk localized Prostate Cancer (HYPO-RT-PC). For complete dose volume constraints, see Table 3.1. The rCT was used as image material for the initial treatment planning and the final treatment plan was recalculated on the sCT and the CT. The rCT plans created were normalized to 100% in PTV mean dose before recalculation on sCT and CT. The plans transferred to the sCT and CT were identical to the plan created on the rCT, with same field setup, and contained the same number of monitor units for each field after final dose calculation. The alignment of the five fields were found to be adequate to meet the dose volume constraints, and the use of five field IMRT for prostate treatment have been described in the work of others (Tomiyama et al., 2014). In Figure 3.3 the final dose distributions for patient case 1 is illustrated.

Table 3.1 Dose volume constraints used for the IMRT treatment planning study. The constraint was used as references when creating the treatment plans, and all plans was optimized to fulfill the constraints. The constraints, presented in both percent and Gy, are used in the conventional arm of the Swedish multicenter Phase III study of HYPO-fractionated Radiotherapy of intermediate risk localized Prostate Cancer (HYPO-RT-PC).

Priority	Volume	Dose volume constraint
1	CTV	$D_{min} \geq 95\%$ $D_{min} \geq 74Gy$
2	PTV	$V_{95\%} \geq 95\%$ $V_{74Gy} \geq 95\%$
3	Rectum	$V_{90\%} \leq 15\%$ $V_{70Gy} \leq 15\%$
4	PTV	$D_{99\%} \geq 90\%$ $D_{99\%} \geq 70Gy$
5	Rectum	$V_{75\%} \leq 35\%$ $V_{59Gy} \leq 35\%$
6	Femoral heads	$D_{max} \leq 70\%$ $D_{max} \leq 55Gy$
7	Rectum	$V_{65\%} \leq 45\%$ $V_{51Gy} \leq 45\%$

8	Body	$D_{max} \leq 105\%$ $D_{max} \leq 82Gy$

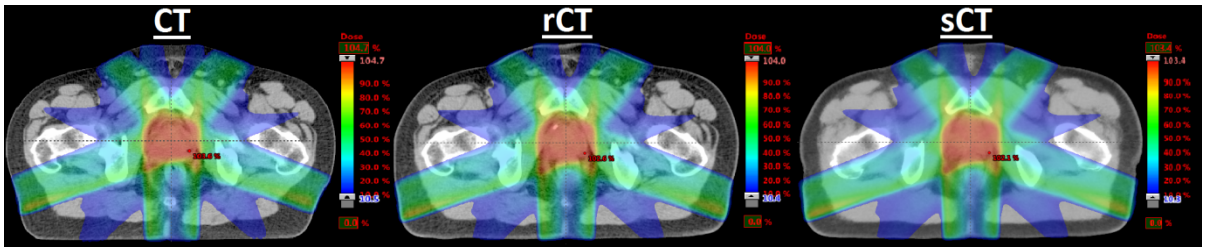

Figure 3.3 Illustration of dose distributions for patient case 1, planned with five 6MV IMRT fields in Eclipse (Varian Medical systems, Palo Alto, CA). The illustration pictures the dose distribution for the created rCT plan and the dose distribution obtained through recalculation on the CT and sCT images respectively.

3.5.2 Proton treatment planning

A spot scanning proton treatment plan was generated for each patient, using the Eclipse treatment planning system (Varian Medical systems, Palo Alto, CA) available at Skandionkliniken. The same structures as for the IMRT treatment planning study was used, although with other CTV *to PTV* margins. The CTV was expanded with 7 mm in all directions to create the PTV; except in the lateral direction were the margins was set to 12 mm. The lateral expansion has been described by Meyer et al. which also uses a similar CTV to PTV expansion in the remaining directions. The margins were used in order to account for proximal and distal range uncertainties and potential setup and motion errors (Meyer et al., 2010). The prescribed dose was 78 Gy with 2 Gy per fraction, with a RBE correction factor of 1.1. Given this, a dose prescription of 70.909 Gy with 1.818 Gy/fraction was specified in the TPS. The PTV margins and the RBE correction factor was consistent with the recommendations from the International Commission on Radiation Units and Measurements No.78 report (ICRU, 2007).

All treatment plans consisted of two opposed lateral beams, with the gantry angled at 90 and 270 degrees, optimized to deliver a uniform dose to PTV using single field optimization. The final dose calculation was made with a pencil beam algorithm (PBA, Proton Convolution Superposition v13.0.28). The same approach as for the IMRT treatment planning was used; creating the initial plan on the rCT with a normalization of 100% in PTV mean dose, following recalculation on the sCT and CT images. The created proton plans were optimized to fulfill the same criteria as the IMRT plans, given in Table 3.1. In Figure 3.4 the final dose distributions for patient case 1 is illustrated.

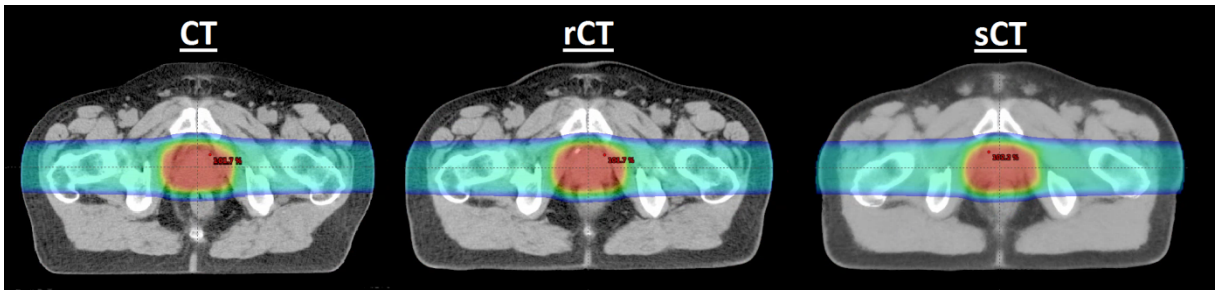

Figure 3.4 Illustration of dose distributions for patient case 1, with a two field proton plan in Eclipse (Varian Medical systems, Palo Alto, CA). The illustration pictures the dose distribution for the created rCT plan and the dose distribution obtained through recalculation on the CT and sCT images respectively.

3.5.3 Dose volume histogram evaluation

For the dose volume histogram (DVH) evaluation process, the rCT was used as the reference. The sCT and the CT plan were compared to the rCT plan, analyzing the mean doses to PTV, CTV, bladder, rectum, femoral heads and the body. Further, the DVH points mentioned in the HYPO-study were also analyzed, see Table 3.1. For extraction of the points of interest, the plan evaluation tool in Eclipse was used in combination with an in-house developed program, based on the Eclipse Scripting API, for parameter extraction.

Differences in absorbed dose between sCT/rCT and CT/rCT plans were determined for each patient, and the mean value and standard deviation (1 s.d.) was calculated for all patients. Due to differences in field of view in the slice direction between the CT and rCT, the Body mean value was excluded from the CT result.

3.5.4 Gamma analysis

In addition to the DVH analysis, a gamma analysis was made for each individual patient comparing the sCT to the rCT dose distribution and the CT to the rCT dose distribution. As described in the theory section (see section 2.3) this gamma analysis was made between two calculated dose matrices. The rCT dose matrix was set as a reference and the CT and sCT dose matrices were used as evaluation distributions.

The gamma analysis was made with an in-house developed MATLAB program. A 2D gamma map was calculated for the isocenter slice, taking into account the nearest slices of the evaluated distributions (i.e. evaluation in all three spatial dimensions). The gamma pass rate was determined for each patient case, both for the sCT/rCT and the CT/rCT comparison. The result for the individual patient evaluation was presented as a bar chart, comparing the sCT/rCT with the CT/rCT analysis expressed as the gamma pass rate. Gamma criteria of 1%/2mm for IMRT and 3%/2mm for protons, local dose deviation, were used. The use of these particular gamma criterions was intended to test the limitations of the used generation method, and discover any possible insufficiencies of the method. The use of a more common criterion, such as 3%/3mm for IMRT, would not give any, or very limited, additional information beyond the DVH-analysis, this since the sCT were expected to be similar to the rCT. All dose criteria express local dose difference.

3.6 Positioning study

A positioning study was conducted to investigate the possibilities of patients positioning in an MRI only workflow. Through examination of the image material available in an MRI only workflow compared to the combined CT/MR workflow, difficulties and possibilities with MRI only positioning strategies was described. A MV bone match procedure was tested and a fiducial marker identification study performed.

The positioning of the patient is a step that important in order to deliver the prescribed treatment. If the patient is incorrect positioned the purpose of the treatment may be lost, since the treatment is constructed with regard to a specific positioning of the patient. In a combined CT/MR workflow for prostate patients, a CT image or a digitally reconstructed radiograph (DRR) works as a reference image for positioning of the patient during the treatment session. This image is matched with an image acquired during the treatment session, which commonly is a cone beam CT (CBCT) image or a pair of mega voltage (MV) or kilo voltage (kV) images. The image match for prostate cancer patients is made either with bones and soft tissue as reference, or with fiducial markers. The CBCT match is performed on bones with the soft tissues as guide, and the CBCT is therefore referred to as a bone and soft tissue match procedure. From the match, a calculated couch travel is acquired, according to which a

movement of the couch can be performed in order to transfer the patient to the right treatment position. In the suggested MRI only workflow the positioning strategies can proceed in the same manner as in the conventional workflow; with the CT replaced with an MRI, sCT or DRR reconstructed from the sCT.

3.6.1 Bone match

In an MRI only workflow the CT-DRR must be replaced with a sCT-DRR when considering a bone match with MV or kV images. This is a matching procedure that can be used for prostate cancer patients with no possibility of fiducial markers (e.g. radical prostatectomy), or the cases where the prostate glands are a part of the CTV. CBCT match with bones is also a common technique for these patients, but not always available. In order to test a bone match procedure, the image material consisting of CT, sCT and MV images were imported into Eclipse. The CT and sCT were rigidly registered to each other, using the bones to achieve the best possible agreement between the images. The two images were placed in the same coordinate system; creating plans with two orthogonal fields, with identical isocenters. This enabled a comparison of the displacement arising from matching the CT-DRR and sCT-DRR against the MV images. If the bones in the CT-DRR and sCT-DRR were identical, equal displacements was expected.

DRRs were created for each field and plan, and the MV images were imported into Aria. The Eclipse Offline review tool was used to test the matching procedure. The images were manually matched to achieve the best possible bone match between the MV images and the CT-DRR and sCT-DRR respectively. The displacement in lateral, longitudinal and vertical direction was noted for both sCT and CT. These results were used for comparison of the two techniques, investigating if an MRI only workflow could position the patients with the same positions as the conventional workflow.

3.6.2 Fiducial marker identification

The fiducial markers were not possible to detect in the T2 weighted images used for sCT generation. This is a problem that the combined MR/CT workflow also has, and in order to detect the markers, an extra MRI set is used for identification. In a combined workflow the identification can be performed with the CT as a reference were the markers should appear. In an MRI only workflow this is not possible, and the extra MRI set must be used on its own. Since the identification of the markers not always is self-evident, a study was carried out to see with which precision the markers could be detected.

The MR set used for identification in the combined workflow (LAVA-flex) was imported into the Eclipse TPS and the contouring tool was used for identification and marking of the fiducial markers. One of the five patients was excluded due to a change in the MR protocol used, resulting in a different MRI sequence for identification of the fiducial markers for this patient. Six observers performed identification of the markers, independently of each other, for each of the remaining four patients. The observers had different experience with fiducial marker identification, but with enough experience to manage the task. Each observer was instructed to mark the right-most marker as the first, the left-most as the second and the marker placed most centered as the third. The marker position was noted for each observer in x-, y- and z-direction, and the result compared within each patient. Each observer was also instructed to grade the degree of confidence, from one to five, which the markers were placed with. The confidence level was dependent on how the observer experienced the identification and the ability to send the patient further to treatment. Only the LAVA-flex set was available for marking, and it was not permitted to use neither the CT nor the other observers' markers as help. In Table 3.2 the confidence grading is described in more detail.

Table 3.2 The different levels of confidence used in the fiducial marker study ranging from one to five. The levels were set with the MRI only workflow in mind and the possibility to pass the patient on further down the workflow as the goal.

Level of confidence	Explanation	
1	**Very doubtful**	**Identification not possible.**
2	**Doubtful**	**Identification deficient;** Patient could not be passed on.
3	**Undetermined**	**Identification possible;** Hesitant decision if the patient could be passed on.
4	**Confident**	**Identification confident;** Patient can safely be passes on, although the images had more to be desired.
5	**Very confident**	**Identification convincing.**

4. Results

4.1 Image evaluation

The image evaluation consisted of a visual evaluation and a DICE calculation. In Figure 4.1 the visualization and DICE calculation for five slices for patient case 2 and 5 are displayed. Patient case 2 had the lowest mean DICE value and patient case 5 had the highest mean DICE value, when considering both sCT/rCT and CT/rCT comparisons. The DICE value was in general lower for the more cranial slices, and the sCT/rCT comparison showed a lower DICE value than the CT/rCT comparison. The mean DICE value for all patients was 87.8% for the sCT/rCT comparison and 92.8% for the CT/rCT comparison. The most visible differences were seen in the bone edges, at the higher parts of femur near the hip joint, and at narrow connective parts of the bones found in the cranial slices. For complete information for each patient case and slice, see Appendix VI and Appendix VII.

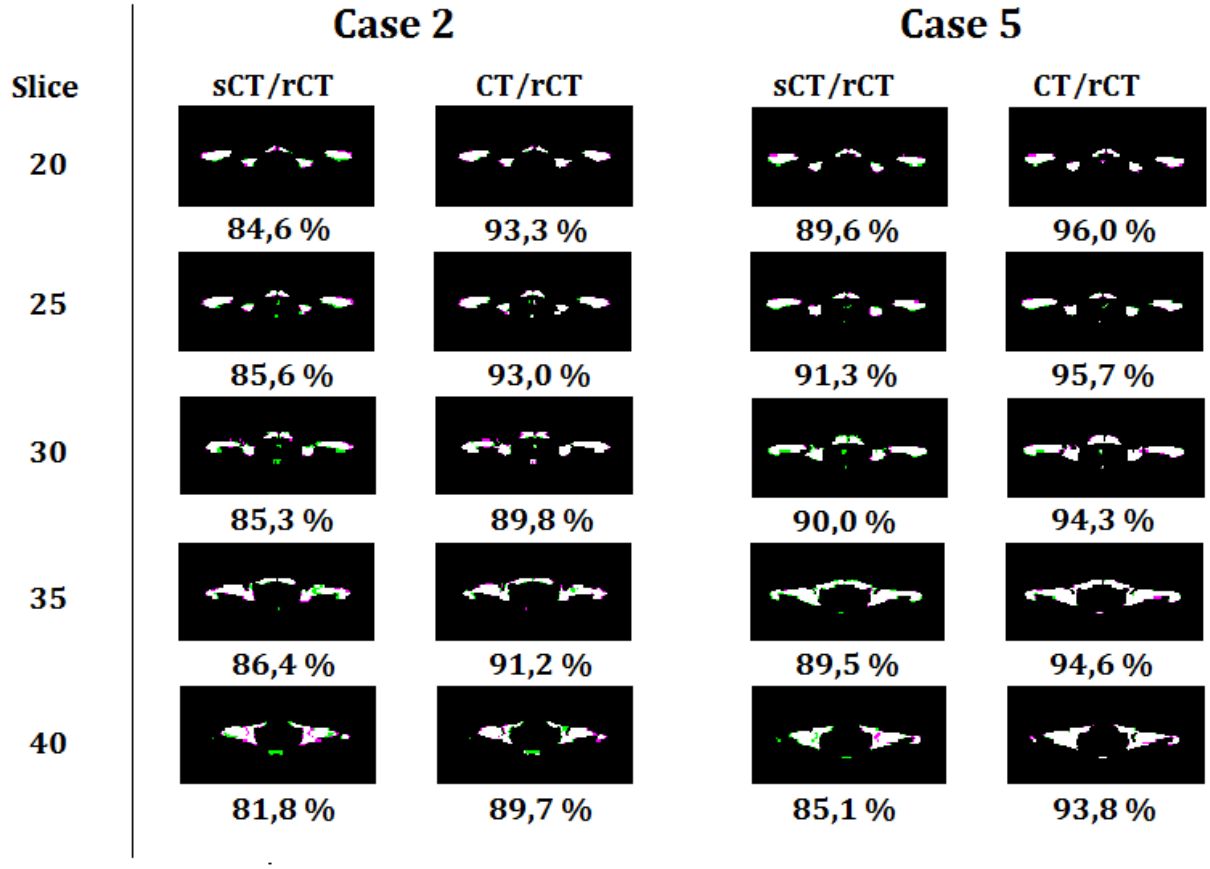

Figure 4.1 The DICE value in five slices for two patients is presented in the above image. The slices ranges from 20 to 40, where 20 is the slice located closest to the feet's and slice 40 located closest to the head of the patients. Pink and green color corresponds to pixels that did not agree in the images, green presents pixels belonging to rCT and the pink the sCT or CT. White areas corresponds to pixels that agrees in the compared images, called overlapping pixels.

4.2 Treatment planning

4.2.1 IMRT treatment planning

Figure 4.2 and Figure 4.3 shows the mean differences in absorbed dose when CT and sCT was compared to the rCT for the six patients evaluated. For the comparison, point doses were evaluated according to the constraints presented in section 3.5.3. The zero mark represents perfect match between the dose/volume points compared, and any deviation from the line pictures a difference. For complete information of each patient case see Appendix I and Appendix II.

The result shows a small deviation between sCT and rCT for all DVH points evaluated. The deviations were below 1%, with a standard deviation ranging between 0.0% to 1.4% for all points and both energies evaluated. The CT/rCT comparison shows larger deviations in general, where the largest deviations can be seen for the bladder and rectum DVH points. The PTV DVH points show for both comparisons high agreement, and is the structure that has the smallest deviations for both comparisons. This result is consistent for both energies evaluated, and in general, a similar result can be seen for all DVH points evaluated. The standard deviation is larger for the CT/rCT comparison, where a standard deviation of approximately 4-5% can be seen for the irradiated rectum volume.

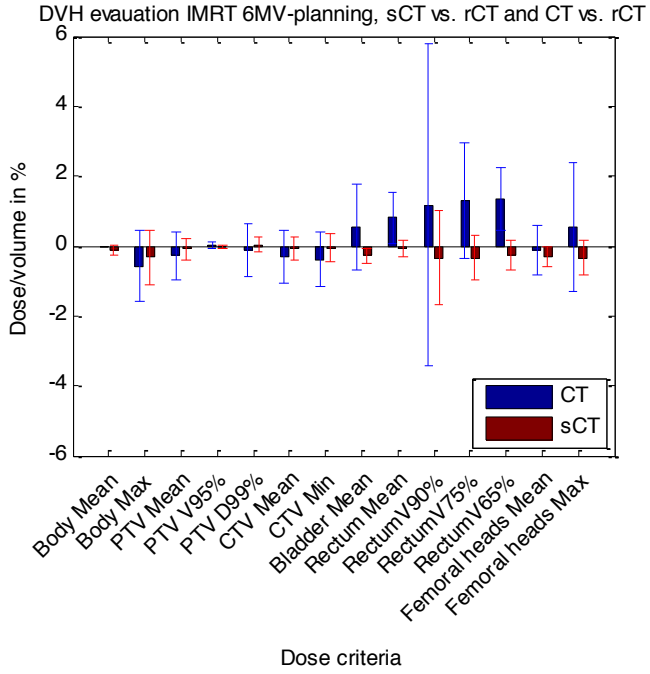

Figure 4.2 The bar chart presents the differences in absolute doses (presented in %) between sCT/r CT, red bars, and CT/rCT, blue bars, for specific organ doses. The evaluation was made for 6MV IMRT. The organs doses are divided into 14 groups, presented on the x-axis, were each group consists of the result from the sCT/rCT and CT/rCT comparison. Each group is presented with its individual standard deviation as error bars (1 s.d.).

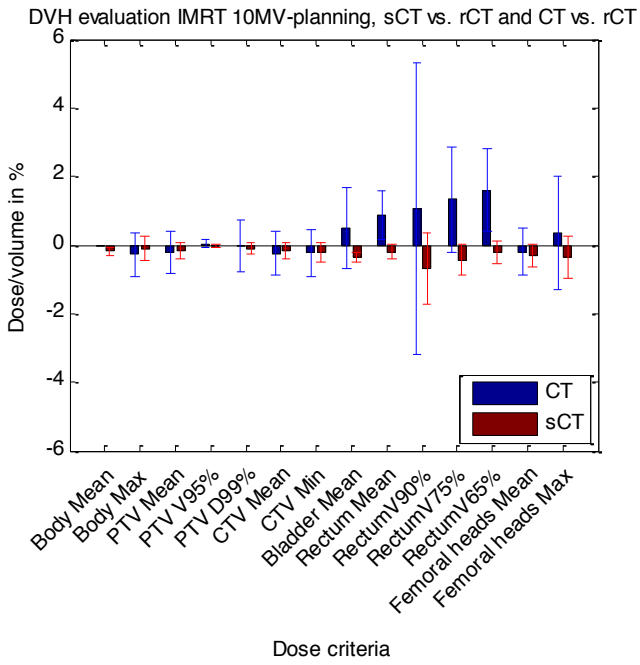

Figure 4.3 The bar chart presents the differences in absolute doses (presented in %) between sCT/r CT, red bars, and CT/rCT, blue bars, for specific organ doses. The evaluation was made for 10MV IMRT. The organs doses are divided into 14 groups, presented on the x-axis, were each group consists of the result from the sCT/rCT and CT/rCT comparison. Each group is presented with its individual standard deviation as error bars (1 s.d.).

The gamma analysis was carried out for each patient case and the resulting gamma map for the isocenter slice is presented in Figure 4.4 and Figure 4.5 for 6 and 10 MV respectively. In this study a five field IMRT setup was used for each patient, and the typical field edges of the five IMRT-fields can be seen as streaks of light blue color in the gamma analysis visualization. This is a result of the dose-calculation on the different images, in which difference can be seen in the field edges.

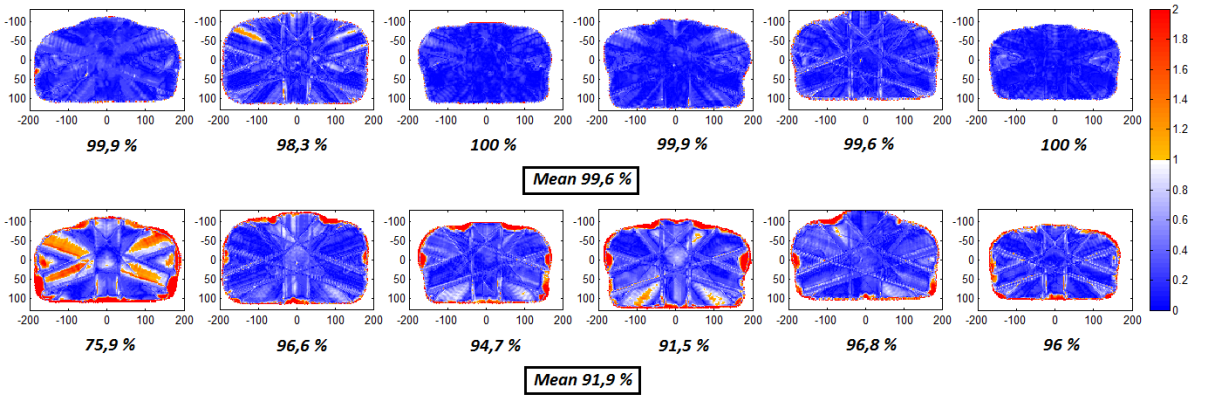

Figure 4.4 The figure illustrates the gamma analysis in 3D for the IMRT 6MV treatment planning. The isocenter slice from the evaluation between sCT/rCT and CT/rCT is shown where the top row presents the sCT/rCT comparison and the bottom row shows the CT/rCT comparison. Points with a value ≤ 1 passes the gamma criterion. Beneath each patient case, the gamma pass rate is presented in percent, and the mean value is presented below each row of patients. The gamma criterion used is 1%/2mm.

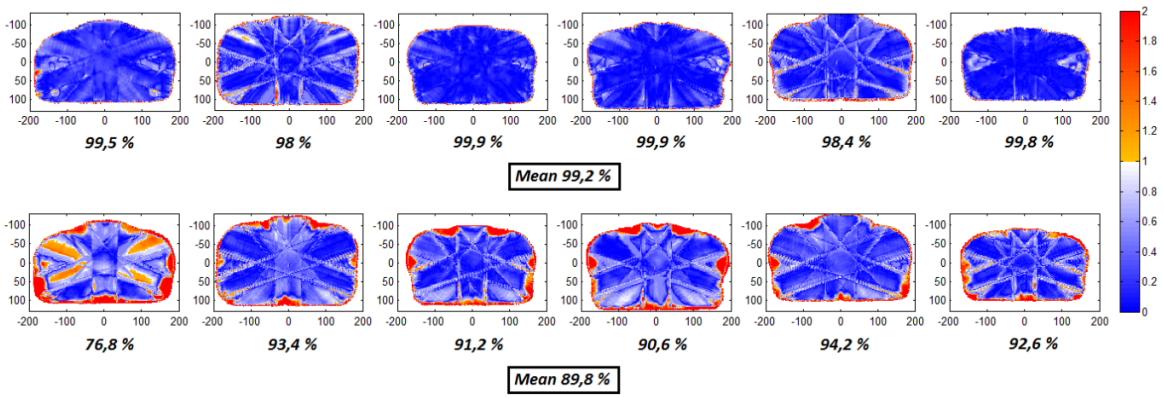

Figure 4.5 The figure illustrates the gamma analysis in 3D for the IMRT 10MV treatment planning. The isocenter slice from the evaluation between sCT/rCT and CT/rCT is shown where the top row presents the sCT/rCT comparison and the bottom row shows the CT/rCT comparison. Points with a value ≤ 1 passes the gamma criterion. Beneath each patient case, the gamma pass rate is presented in percent, and the mean value is presented below each row of patients. The gamma criterion used is 1%/2mm.

4.2.2 Proton treatment planning

Figure 4.6 shows the DVH evaluation bar chart resulting from the dose point evaluation of the proton treatment plans for the six patients included in the treatment planning study. The comparison was made in the same manner as the IMRT DVH evaluation and the bar chart presented below presents the mean differences in absorbed dose when CT and sCT was compared to rCT.

Mean absorbed dose differences for the proton CT/rCT comparison was $-0.3 \pm 0.2\%$ (1 s.d.) for PTV, $-0.1 \pm 0.1\%$ (1 s.d.) for CTV, $3.0 \pm 6.6\%$ (1 s.d.) for the bladder and $-1.1 \pm 4.0\%$ (1 s.d.) for rectum. The corresponding differences in mean absorbed doses for the sCT/rCT comparison were $-0.1 \pm 0.2\% - 0.1 \pm 0.1\%$, $-0.0 \pm 0.6\%$ and $-0.3 \pm 0.6\%$ (1 s.d.) for PTV, CTV, bladder and rectum respectively. For complete information of each patient case, see Appendix III.

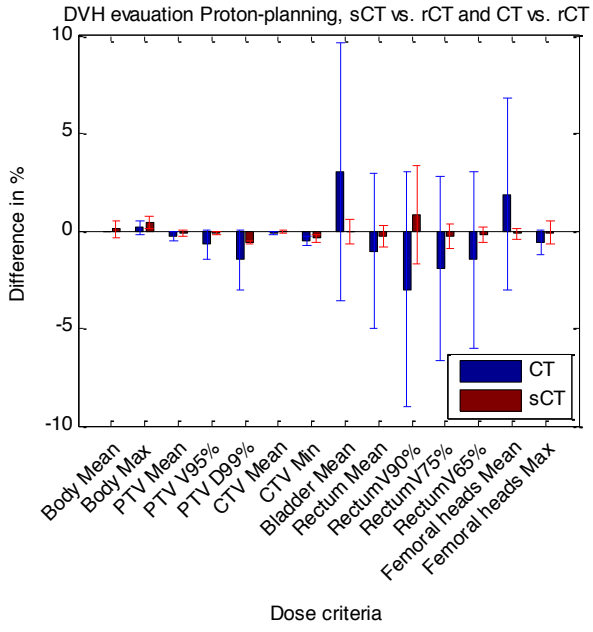

Figure 4.6 The bar chart presents the differences in absolute doses (presented in %) between sCT/r CT, red bars, and CT/rCT, blue bars, for specific organ doses. The evaluation was made for protons. The organs doses are divided into 14 groups, presented on the x-axis, were each group consists of the result from the sCT/rCT and CT/rCT comparison. Each group is presented with its individual standard deviation as error bars (1 s.d.).

In Figure 4.7 the gamma evaluation between sCT/rCT and CT/rCT dose distributions is shown for the proton treatment planning. The top row presents the sCT/rCT comparison and the bottom row presents the CT/rCT comparison. The appearance differs from the IMRT treatment planning in the way that a larger zero dose area is present, which in the illustration can be seen as white area surrounding the dose distribution.

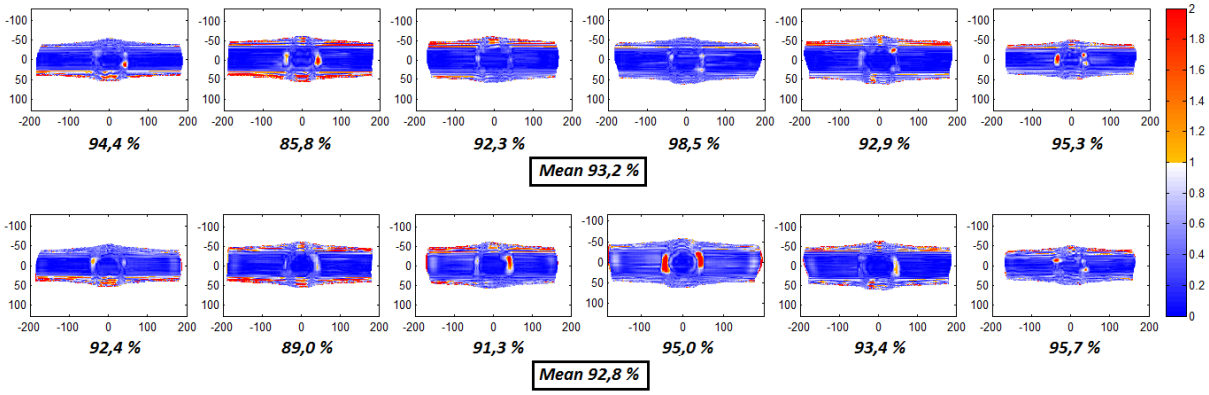

Figure 4.7 The figure illustrates the gamma analysis in 3D for the proton treatment planning. The isocenter slice from the evaluation between sCT/rCT and CT/rCT is shown where the top row presents the sCT/rCT comparison and the bottom row shows the CT/rCT comparison. Points with a value ≤ 1 passes the gamma criterion. Beneath each patient case, the gamma pass rate is presented in percent, and the mean value is presented below each row of patients. The gamma criterion used is 3%/2mm.

4.3 Positioning study

4.3.1 Bone match

The result from the bone match study is presented in Table 4.1. The displacements arising from the positioning against orthogonal MV images is presented in mm for sCT and CT match and the difference between these matches are presented. The displacement is presented in the vertical (Vrt), longitudinal (Lng) and lateral (Lat) directions for each patient, matched for one treatment session. The difference between sCT and CT displacements for all five patients is presented in three directions, where the mean difference in all directions is below 1 mm.

Table 4.1 The positioning study was performed with bone match for 5 patients for both CT and sCT images, matched against two orthogonal MV images from one treatment session. The results are presented in mm displacement, achieved when the images were matched in Eclipse offline-review. The displacements are presented in the vertical (Vrt), longitudinal (Lng) and lateral (Lat) directions. Differences between the displacement for the CT and sCT image match are presented to the right in the three directions in mm.

		Displacement sCT [mm]	Displacement CT [mm]	Difference (sCT-CT) [mm]
Patient 1	Vrt	-2.7	-3.4	0.7
	Lng	-21.4	-20.9	-0.4
	Lat	16.8	18.0	-1.2
Patient 2	Vrt	-11.9	-11.7	-0.2
	Lng	-3.5	-2.8	-0.7
	Lat	13.0	14.0	-1.0
Patient 3	Vrt	-6.9	-5.7	-1.2
	Lng	9.2	7.9	1.4
	Lat	0.1	0.1	0.0
Patient 4	Vrt	-10.4	-10.2	-0.2
	Lng	1.9	1.1	0.8
	Lat	13.5	14.2	-0.7
Patient 5	Vrt	12.1	10.8	1.3
	Lng	-3.1	-4.1	1.0
	Lat	10.8	11.1	-0.3

The mean differences between the displacement achieved from the sCT and CT bone match were 0.7 mm in the vertical direction, 0.9 mm in the longitudinal direction and 0.7 mm in the lateral direction.

4.3.2 Fiducial marker identification

The fiducial marker identification was performed independently by six observers, for four patients. The result is presented in Table 4.2 as the mean standard deviation in x-, y- and z-direction for each marker and patient resulting from the identification of the six observers. One marker identification result for patient 2 was excluded due to an incorrect identification by one observer. See Appendix IV for complete information of the individual observer identifications, and specific information of the standard deviations in respective direction.

The result showed that the fiducial markers could potentially be identified, but not in its correct position in x-, y- and z-direction. The highest standard deviation, in all directions, was 3 mm and the confidence level that the observers experienced ranged between 2 and 5 for all patients. For complete information of the markers positions for each observer, see Appendix IV and Appendix V.

Table 4.2 The fiducial marker identification is presented as the mean standard deviation in x, y and z direction for each marker and patient. The mean standard deviation is presented in mm deviation of the location of the markers, identified by the six observers. The certainty level is presented for the six observers for each patient, from the smallest to the highest level chosen.

Patient	Marker	Standard deviation (x, y, z) [mm]	Confidence level
Patient 1	1	0.3	3-4
	2	1.1	
	3	0.2	
Patient 2	1	0.7	2-3
	2	0.1	
	3	0.6	
Patient 3	1	0.1	2-4
	2	0.1	
	3	0.5	
Patient 4	1	3.0	4-5
	2	0.2	
	3	0.5	

5. Discussion

5.1 Image evaluation

The image evaluation consisted of a visualization of the differences in the bony structures of the images and a calculation of the Dice similarity index. The differences were expected to be found at the bone surfaces, since the generation of the sCT depends on an MRI without strict information of the bones positions. When the images were overlaid in MATLAB, differences could be seen although these were relatively small. Overall the CT and rCT images agreed better than the sCT and rCT. The rCT and CT bone structures are expected to be very similar since it's merely a registration of the CT to the MR, during which the bones did not deform, that differs between the rCT and the CT. The registration shows potential patient repositioning between the MRI and the CT. Repositioning effects can be expected to occur in the outer body contours and in the bladder and rectum volume, which are volumes that easily moves and are hard to reproduce exactly in position. But the bones are relatively stable in their positions and therefore expected to be fairly the same between the imaging sessions. This assumption is further strengthened by the feet immobilization and knee support used when the patients are positioned, enabling reproduction of the bones positions.

The Statistical Decomposition algorithm generates sCTs with the bones in similar positions as the rCT, with small differences in the bone contours and in the connective areas of the bones; as seen in Figure 4.1. This is likely an effect of the sCT generation method, which relies upon the MRI and therefore a precise CT copy is not likely to be expected. An additional aspect that could influence the result is the blurred appearance of the sCT compared to the rCT and CT. This blurring effect arises from the sCT generation and is mostly present in areas with large contrasts/HU differences, for instance in the proximity between soft tissue and bone. This can be troublesome when a threshold is used to segment the bones. The differences presented and calculated in the images are dependent on the threshold used to segment the bones in the images, since this decides how much bone to incorporate in the bone structures. The DICE similarity index gives an indication of the similarities in the images, where a greater agreement can be seen between the CT/rCT compared to the sCT/rCT. The DICE index was in general lower for the cranial slices compared to the caudal slices. The cranial slices consist of more complex bone structures and also narrower connective areas, where the blurring effect can result in absence of bone structures when a threshold is set. This contributes to a lower DICE index.

5.2 Treatment planning

The treatment planning procedure is an essential part of the radiotherapy chain, and is an important step in order to provide safe and accurate treatments. When introducing an MRI only radiotherapy chain, the sCT must provide equal treatment plan quality and accuracy as when a CT is used as image material. A high accuracy have been shown for RapidArc treatment planning using the SDA method for prostate patients (Siversson et al., 2015), and to further test the feasibility of the method, a set of IMRT- and proton treatment plans was produced and evaluated.

As can be seen in Figure 4.2, Figure 4.3 and Figure 4.6, the differences in mean absorbed doses between the sCT and the rCT were in general smaller than between the CT and rCT. This indicates that the doses calculated by the treatment planning system (TPS) based on sCT and on rCT are in better agreement with each other than those calculated based on the CT. Although differences can be seen, these are small and for the sCT/rCT comparison the differences were approximately negligible when compared to the overall dose accuracy needed in radiotherapy, where literature suggests 2.5-3.5% (IAEA, 2000, Brahme, 1984, Goitein, 1983, Mijnheer et al., 1987). This shows that

uncertainties, in terms of absorbed doses, introduced by treatment planning on sCT generated by the SDA method are negligible, and the resulting dose to target and risk organs are practically the same. This is independent of the modality used and the same trend can be seen for the IMRT and proton plans.

The differences between the dose distributions are more distinct for the CT/rCT comparison, which can be seen both in the DVH- and the gamma analysis. The larger differences between CT and rCT are probably an effect of repositioning between MR and CT. This can be seen as uncertainties introduced by repositioning between MR and CT in a combined workflow, which is one of the main concerns regarding the combined MRI/CT workflow. This is illustrated in Figure 4.4 and Figure 4.5, where the bottom row can be seen to have a larger number of non-passing points between the distributions evaluated. Differences can mostly be seen in the edges of the distributions, where the effect of the repositioning is mostly present.

The gamma analysis was used to test if the use of sCT images generated from the SDA method resulted in any deficiencies in the resulting dose distribution, when compared to rCT. The result showed that the dose distributions resulting from the IMRT treatment planning on the sCT and the rCT are in very good agreement with each other. When the treatment plan is recalculated on the CT and sCT, the dose planning system must take into account the new structures and geometries of the new images, which in this study is the sCT and CT, since the original plan was created on the rCT. These three images, rCT, sCT and CT, are supposed to be similar, although some disparities are expected to be found. The disparities result in various dose distributions, which in a wide perspective is found to be very similar. For example are the absorbed doses to the inner structures as PTV, bladder and rectum relatively unaffected. At the field edges the differences seems to be of larger extent, which contributes to the calculation not passing the gamma evaluation completely at all evaluation points.

The DVH analysis of the proton plans showed a larger deviation between the rCT and CT plan than showed for the IMRT plans. The protons are more sensitive to the position of structures, and the differences that can be detected in rectum and bladder volume results in a larger deviation when the rCT and CT plans are compared. A larger difference can also be seen in the femoral heads; which also is a result of the more sensitive behavior of the protons. However, the sCT/rCT comparison showed, regardless of the larger deviation between CT/rCT, a good agreement. The proton gamma analysis resulted in lower pass rate than the IMRT evaluation. The gamma criterion was eased in order to identify the areas with largest differences in calculation results. The protons more sensitive range properties influenced the gamma evaluation, and the pass rate was lower than for the photons. The mentioned blurring effect in the image analysis become visible in the gamma analysis, and a streak of red non-passing points could be seen in similar positions as where the bone contours differed in the image analysis. Regardless of this fact, the proton treatment plan would, according to the clinical criteria used in this work, be acceptable.

In this study, the same structures were used in all datasets. Another option would have been to create new structures on each image. However, this would have required different treatment plans for each image which would be a drawback when comparing the calculated dose distributions. The method used in the study enables comparison of volumes of the same size and position, but can result in a structure volume that does not agree with the CT. The structure outlined on the MR should agree with both sCT and rCT, but the CT can be different due to reposition between imaging sessions. This in turn enables investigation of the repositioning effects, as shown in the study.

5.3 Positioning study

The aim of the positioning study was to investigate positioning possibilities in an MRI only workflow and to detect possible difficulties. The suggested workflow was followed, in which bone match or fiducial marker match was the suggested techniques for prostate cancer patients, when considering a workflow without the possibility of a matching procedure with MR.

The bone match was performed with MV images and resulted in a mean difference below 1 mm when the CT and sCT match displacements was compared. This result indicates that despite the small bone differences that could be seen in the image evaluation, the matching could work in the same manner in the MRI only workflow as in the conventional workflow. The differences ranged in mean values between 0.7-0.9 mm in all directions, where the smallest deviation was 0.0 mm and the largest 1.4 mm. The result is dependent on the operator that performs the match, and the operator's experience is important for the continuation in developing positioning strategies. The initial experience from this study was that the sCT and CT could be matched in similar ways to the MV images, and no significant difference in the matching procedure was detected. The bone match with MV or kV images is not always the preferred method for prostate cancer patients. Due to daily variations in prostate placement and soft tissue, it is preferred to do either a CBCT or a fiducial marker match to encounter such variations. Despite this, the bone match can be preferred for other diagnosis such as head and neck cancers where soft tissue movement is a smaller concern. The use of fiducial markers in the prostate enables to encounter the daily variations in position of the prostate, and the use of fiducial marker match is a modality that needs further consideration in the MRI only workflow.

The fiducial marker identification study in this thesis aimed to test the concept of the fiducial marker positioning strategies that are used in the conventional workflow for prostate patients. Early on it was clear that the markers was hard to identify exactly in the LAVA-flex MR images that were available. This resulted in an observer study that tested the precision that the markers could be identified with and the observers experienced confidence regarding the identification. The study showed that the markers in most cases could be identified with good precision, except in one case were a marker was identified far off from the correct position. The actual patient case had small air cavities or calcifications in the prostate that confused the observers. This resulted in a confidence level between 2 and 3, which would result in this patient not being passed on to treatment. The misplaced marker was identified in the position of an air cavity or calcification that easily could be mistaken for as a marker. The main experience from the observers was that the markers were hard to identify, but the task was feasible. This is a problem that needs to be addressed, and the use of sequences with better identification possibilities is essential for the continuation of fiducial marker positioning in the MRI only workflow. Alternative marker materials are also an alternative that could improve the identification possibility. Alternative markers have been tested for the conventional workflow (Habermehl et al., 2013); the identification feasibility of these markers on an MRI would be an interesting study.

5.4 Summary

The parts of the workflow investigated in this thesis are strongly connected. The image evaluation hypothesis was that the bone contours were expected to be hard to reproduce in a synthetic CT, which to some extent were found to be adequate. The segmented bone structures were not identical between the sCT and rCT. This was expected to be translated in to the treatment planning result, were the larger attenuation properties of the bones were expected to lead to larger disparities between the sCT and rCT dose distributions. This was not the case. Even though differences between sCT and rCT could be observed, and calculated with the DICE index, the evaluated DVH points were comparable for the plans. This indicates that an exact bone agreement is not necessary for creating comparable dose plans for the DVH points evaluated in this work. The DICE index should not be an exclusive measure on whether or not a generation method could be integrated in the MRI only workflow. But the DICE index could be used to evaluate how different generation methods works and compares, in order to detect advantaged and difficulties in generation methods. A good agreement in the bone positions of a generated synthetic CT and the original CT is always preferable, but the question is to which extent the images must agree in order to create comparable dose distributions? From this study we can see that despite disparities in the bone surfaces of the sCT and rCT, the resulting dose distributions were comparable to a very high degree. Small differences do not influence the result distinct for the photons, but the protons shows a more sensitive behavior to these disparities.

Positioning strategies in an MRI only workflow is a fairly unexplored area, and from this thesis it can be concluded that this part of the workflow needs to be carefully further studied. Focuses of researchers has been on creating and developing different generation methods, in order to have an operating dose planning foundation. This is an important step towards an MRI only workflow, but in order to enable a complete MRI only workflow, more insight in the positioning strategies is needed. This study was limited by time and availability of patient material, but the work done indicates an interesting future with further investigations on positioning strategies.

A consistent concern when investigating MRI only is the uncertainties that are introduced by the different steps involved in MRI only. This thesis showed that treatment planning on sCT introduced a mean dose difference to PTV of -0.1% (6MV), -0.2% (10MV) and -0.1% (protons) when comparing sCT and rCT. In the context of overall dose accuracy, the uncertainty contribution from dose planning on sCTs generated from the SDA seems negligible. When considering introducing uncertainties, it is also important to remember that the MRI only workflow is intended to eliminate uncertainties. Nyholm et al. states that the MRI only workflow reduces geometrical uncertainties with 1-2 mm when compared to a combined CT/MR workflow for prostate patients (Nyholm et al., 2009). The bone positioning study in this work showed a mean difference of 0.7-0.9 mm between sCT and CT bone match. If compared to the uncertainties eliminated through exclusion of the co-registration process, this additional contribution of uncertainty seems acceptable. The differences between the sCT and CT match does not solely depend on that the sCT is synthetic, the rigid registration of the CT and sCT influences the result. In the actual study only one observer performed the match, which also influences the result.

The MRI only workflow has many steps that could introduce random and systematic errors, and all of them are not possible to handle in this work. Geometrical distortions are a concern that commonly is mentioned along with MRI-based radiotherapy as one of the main challenges (Korsholm et al., 2014), and are a phenomenon that can influence the clinical outcome of the treatment (Walker et al., 2014). The distortions can be caused both by the system used for imaging, but can also be patient dependent. Even though this is a common concern in MRI only, there are works describing methods to reduce the distortions (Crijns et al., 2011). The possible alternative to the combined MR/CT workflow for

prostate patients has its difficulties, but also shows promising results. The MRI only workflow cannot completely replace the CT/MR workflow at the present time, but the field is fast developing and the technique shows a promising future.

It is important to understand not only the possibilities but also the concerns with the MRI only workflow. The use of smaller margins is often mention as a positive effect of the use of MR, but reduced margins can also lead to deficit of dose to PTV if the prostate moves during treatment. A possibility of increasing the dose to the target can be possible with decreased margins. OARs can be avoided and a high dose to target can be delivered at the same time as side effects are avoided. This can be a positive effect but if the patient moves during treatment an unwanted high dose can be delivered to an OAR.

6. Conclusion

The dose planning study showed good agreement between the resulting dose distributions arising from dose planning on sCT and rCT for all treatment modalities tested (i.e. 6 and 10 MV IMRT and spot scanning protons), which indicates that SDA generated sCT images can be used in an MRI only workflow. The image evaluation indicated some disparities in the bone surface between sCT and rCT, but this had only small effect on the resulting dose distributions for photon plans. The proton plans indicated a larger sensitivity on the differences in bone contours. To evaluate the usability of a sCT in an MRI only workflow it's vital to evaluate the outcome of the treatment, and to ensure that the prescribed treatment is delivered as when a CT is used. The positioning strategies in the MRI only workflow represent a part of the workflow that needs to be further investigated. The initial results of this study show a problem with transferring the fiducial marker positioning strategies in the conventional workflow to the MRI only workflow. The markers cannot be convincingly identified using the sequence investigated. The bone match can be performed and this is a matching procedure that likely can be usable in the MRI only workflow.

7. Future perspective

The main limitation in this thesis was the limited time and available patient material. Further work is needed in order to incorporate an MRI only workflow in the radiotherapy clinic. This work did only investigate one generation method in one anatomical site, which leaves room for further studies with larger patient selections and multiple generation methods. The investigation of different generation methods can result in improvements in the available methods, but also enable evaluation methods that can be used for comparison. The different generation methods focus on different sites and techniques, and a fair evaluation method for comparison is needed in order to move further when comparing different methods.

The image analysis implicated interesting findings that could be further investigated. The mentioned blurring effect is a possible effect from the SDA generation and further work with the generation method can result in possible improvements. An improvement of the images, that already shows promising treatment planning results, can result in even better results that could further favor the use of MRI in radiotherapy.

As mentioned in the discussion and conclusion, the MRI only positioning strategies need further studies. The desire to find and develop positioning guidelines in the new workflow is an important task that demands larger observer groups and an extended patient selection. The bone match study would preferably be performed with larger patient selections, with different anatomical sites. In order to reduce the influence of the observer, a multiple observer study, as for the marker identification, would be interesting. The marker study showed that even though the markers could be identified, the observer did not feel confident of the marker positions for all patients. This is an issue that comes in early in the chain, and the development of better sequences which leads to more confident marker identifications could likely have a positive effect on the whole workflow. Bone match is not always the preferred matching procedure for prostate patients, and it can often be desirable to locate soft tissue in the matching images. Procedures that enable this would be of interest for investigation, such as CBCT match with bones and soft tissue and ultimately a solely soft tissue match with MRI.

When considering the MRI only workflow, it is important to see the complete workflow from end to end and not only focus on individual steps in the workflow. In order to incorporate MRI in radiotherapy, the whole chain must be connected and stable in order to reach the ultimate goal – a safe, reliable and successful treatment.

8. Acknowledgements

First of all I would like to thank my supervisors, Fredrik Nordström, Carl Siversson and Crister Ceberg.

- Fredrik, I am deeply grateful for having you as my head supervisor. You have guided me through the thesis with grand enthusiasm and encouraged me to develop my own ideas.
- Carl, your faith in the project has been highly appreciated and your critical eye helped me to investigate my work with a different approach.
- Crister, you have always been available for discussion and your thoughts and ideas have been very appreciated throughout the work.

A special thanks to Spectronic Medical AB and their wonderful team that supported me throughout the work. Thank you for welcoming me into your world of programming, your explanations and help, despite my lack of knowledge in your field. Without you this project would not have been possible.

I would also like to thank Umeå University for their contribution and patient material. Special thanks to Jocke and Tufve who has participated as support through the project.

Thanks to the observers that participated in the observer study. Christian, André, Gabriel and Sofie – you took time from your own work to participate in my study, and for that I am grateful.

Thanks to my co-worker students, Minna and Rrezarta. I will remember the times of joy and look back at this with happiness - we finally did it!

Last but not least, thanks to my wonderful family - you have always supported me in my decisions, and encouraged me to press forward.

Lund, May 22 2015
Emilia Persson

9. References

ANDREASEN, D., VAN LEEMPUT, K., HANSEN, R. H., ANDERSEN, J. A. & EDMUND, J. M. 2015. Patch-based generation of a pseudo CT from conventional MRI sequences for MRI-only radiotherapy of the brain. *Med Phys,* 42**,** 1596.

BRAHME, A. 1984. Dosimetric precision requirements in radiation therapy. *Acta Radiol Oncol,* 23**,** 379-91.

CANCERFONDEN. 2015. *Strålbehandling* [Online]. [Accessed 19 February 2015].

CRIJNS, S. P., RAAYMAKERS, B. W. & LAGENDIJK, J. J. 2011. Real-time correction of magnetic field inhomogeneity-induced image distortions for MRI-guided conventional and proton radiotherapy. *Phys Med Biol,* 56**,** 289-97.

DEBOIS, M., OYEN, R., MAES, F., VERSWIJVEL, G., GATTI, G., BOSMANS, H., FERON, M., BELLON, E., KUTCHER, G., VAN POPPEL, H. & VANUYTSEL, L. 1999. The contribution of magnetic resonance imaging to the three-dimensional treatment planning of localized prostate cancer. *Int J Radiat Oncol Biol Phys,* 45**,** 857-65.

DICE, L. A. 1945. Measures of the Amount of Ecologic Association Between Species. *Ecology,* 26**,** 297-302.

DOWLING, J. A., LAMBERT, J., PARKER, J., SALVADO, O., FRIPP, J., CAPP, A., WRATTEN, C., DENHAM, J. W. & GREER, P. B. 2012. An atlas-based electron density mapping method for magnetic resonance imaging (MRI)-alone treatment planning and adaptive MRI-based prostate radiation therapy. *Int J Radiat Oncol Biol Phys,* 83**,** e5-11.

GOITEIN, M. 1983. Nonstandard deviations. *Med Phys,* 10**,** 709-11.

HABERMEHL, D., HENKNER, K., ECKER, S., JAKEL, O., DEBUS, J. & COMBS, S. E. 2013. Evaluation of different fiducial markers for image-guided radiotherapy and particle therapy. *J Radiat Res,* 54 Suppl 1**,** i61-8.

HYPO-RT-PC. *Phase III study of HYPO-fractionated radiotherapy of intermediate risk localised prostate camcer* [Online].

IAEA, I. A. E. A. 2000. Technical report series no. 398: Absorbed dose detemination in external beam radiotherapy - an international code of practice for dosimetry based on standards of absorbed dose to water. .

ICRU 2007. ICRU REPORT No. 78. Prescribing, Recording, and Reporting Proton-Beam therapy

JOHANSSON, A., KARLSSON, M. & NYHOLM, T. 2011. CT substitute derived from MRI sequences with ultrashort echo time. *Med Phys,* 38**,** 2708-14.

JONSSON, J. H., AKHTARI, M. M., KARLSSON, M. G., JOHANSSON, A., ASKLUND, T. & NYHOLM, T. 2015. Accuracy of inverse treatment planning on substitute CT images derived from MR data for brain lesions. *Radiat Oncol,* 10**,** 13.

JONSSON, J. H., JOHANSSON, A., SODERSTROM, K., ASKLUND, T. & NYHOLM, T. 2013. Treatment planning of intracranial targets on MRI derived substitute CT data. *Radiother Oncol,* 108**,** 118-22.

KARLSSON, M., KARLSSON, M. G., NYHOLM, T., AMIES, C. & ZACKRISSON, B. 2009. Dedicated magnetic resonance imaging in the radiotherapy clinic. *Int J Radiat Oncol Biol Phys,* 74**,** 644-51.

KORHONEN, J., KAPANEN, M., KEYRILAINEN, J., SEPPALA, T. & TENHUNEN, M. 2014. A dual model HU conversion from MRI intensity values within and outside of bone segment for MRI-based radiotherapy treatment planning of prostate cancer. *Med Phys,* 41**,** 011704.

KORSHOLM, M. E., WARING, L. W. & EDMUND, J. M. 2014. A criterion for the reliable use of MRI-only radiotherapy. *Radiat Oncol,* 9**,** 16.

LAGENDIJK, J. J., RAAYMAKERS, B. W., VAN DEN BERG, C. A., MOERLAND, M. A., PHILIPPENS, M. E. & VAN VULPEN, M. 2014. MR guidance in radiotherapy. *Phys Med Biol,* 59**,** R349-69.

LAMBERT, J., GREER, P. B., MENK, F., PATTERSON, J., PARKER, J., DAHL, K., GUPTA, S., CAPP, A., WRATTEN, C., TANG, C., KUMAR, M., DOWLING, J., HAUVILLE, S., HUGHES, C., FISHER, K., LAU, P., DENHAM, J. W. & SALVADO, O. 2011. MRI-guided prostate radiation therapy

planning: Investigation of dosimetric accuracy of MRI-based dose planning. *Radiother Oncol,* 98**,** 330-4.

LOW, D. A., HARMS, W. B., MUTIC, S. & PURDY, J. A. 1998. A technique for the quantitative evaluation of dose distributions. *Med Phys,* 25**,** 656-61.

MEYER, J., BLUETT, J., AMOS, R., LEVY, L., CHOI, S., NGUYEN, Q. N., ZHU, X. R., GILLIN, M. & LEE, A. 2010. Spot scanning proton beam therapy for prostate cancer: treatment planning technique and analysis of consequences of rotational and translational alignment errors. *Int J Radiat Oncol Biol Phys,* 78**,** 428-34.

MIJNHEER, B. J., BATTERMANN, J. J. & WAMBERSIE, A. 1987. What degree of accuracy is required and can be achieved in photon and neutron therapy? *Radiother Oncol,* 8**,** 237-52.

NYHOLM, T., NYBERG, M., KARLSSON, M. G. & KARLSSON, M. 2009. Systematisation of spatial uncertainties for comparison between a MR and a CT-based radiotherapy workflow for prostate treatments. *Radiat Oncol,* 4**,** 54.

PARKER, C. C., DAMYANOVICH, A., HAYCOCKS, T., HAIDER, M., BAYLEY, A. & CATTON, C. N. 2003. Magnetic resonance imaging in the radiation treatment planning of localized prostate cancer using intra-prostatic fiducial markers for computed tomography co-registration. *Radiother Oncol,* 66**,** 217-24.

SIVERSSON, C., NORDSTRÖM, F., NILSSON, T., NYHOLM, T., JONSSON, J., GUNNLAUGSSON, A. & OLSSON, L. E. 2015. MRI only prostate radiotherapy planning using the statistical decomposition algorithm (Accepted for publication in Medical Physics). *Med Phys*.

TOMIYAMA, Y., ARAKI, F., OONO, T. & HIOKI, K. 2014. Three-dimensional gamma analysis of dose distributions in individual structures for IMRT dose verification. *Radiol Phys Technol,* 7**,** 303-9.

WALKER, A., LINEY, G., METCALFE, P. & HOLLOWAY, L. 2014. MRI distortion: considerations for MRI based radiotherapy treatment planning. *Australas Phys Eng Sci Med,* 37**,** 103-13.

Appendix I - DVH parameters for IMRT treatment plans.

6 MV IMRT treatment planning results for each patient case. The result from the DVH comparison between the rCT and the CT and sCT, respectively, is shown in the table below.

	Case 1		Case 2		Case 3		Case 4		Case 5		Case 6	
	CT	**sCT**	**CT**	**sCT**	**CT**	**sCT**	**CT**	**sCT**	**CT**	**sCT**	**CT**	**sCT**
Body												
Mean	N/A	-0.3	N/A	0.1	N/A	-0.2	N/A	-0.1	N/A	-0.1	N/A	0.0
Max	0.7	-0.9	-1.2	0.6	0.2	0.0	-2.2	-1.4	-0.6	-0.4	-0.3	0.3
PTV												
Mean	1.0	-0.4	-0.8	0.4	-0.3	-0.2	-0.8	-0.3	-0.6	-0.2	-0.1	0.2
V95%	0.2	-0.1	0.0	0.0	0.0	0.0	0.0	0.0	0.0	0.0	0.0	0.0
D99%	1.4	-0.3	-0.8	0.2	-0.3	0.1	-0.4	0.1	-0.5	-0.1	-0.2	0.3
CTV												
Mean	1.1	-0.5	-0.8	0.4	-0.4	-0.1	-1.0	-0.3	-0.6	-0.2	-0.1	0.2
Min	1.1	-0.7	-0.7	0.2	-0.7	-0.1	-1.1	-0.2	-0.6	-0.1	-0.3	0.5
Bladder												
Mean	-1.2	-0.2	1.4	-0.3	1.2	-0.6	0.2	-0.4	2.0	-0.2	-0.5	0.0
Rectum												
Mean	1.5	-0.5	1.5	0.3	-0.2	-0.1	0.2	-0.1	1.3	0.0	0.6	0.0
V90%	10.3	-2.6	0.6	1.6	-1.2	-0.3	-1.1	-0.2	-2.2	-0.4	0.7	-0.1
V75%	4.5	-1.3	1.5	0.3	0.3	-0.3	0.9	-0.9	-0.1	0.2	0.8	0.0
V65%	2.9	-0.9	1.8	-0.5	0.8	-0.3	1.6	-0.1	0.8	0.3	0.4	0.0
Femoral heads												
Mean	-0.1	-0.3	-0.9	-0.7	1.0	-0.6	-0.9	-0.2	0.0	-0.1	0.1	0.0
Max	4.1	-0.3	-0.9	-0.5	-0.1	-0.8	1.0	0.5	-0.8	-0.8	0.0	-0.1

Appendix II - DVH parameters for IMRT treatment plans.

10 MV IMRT treatment planning results for each patient case. The result from the DVH comparison between the rCT and the CT and sCT, respectively, is shown in the table below. Results presented in percent.

	Case 1		Case 2		Case 3		Case 4		Case 5		Case 6	
	CT	**sCT**	**CT**	**sCT**	**CT**	**sCT**	**CT**	**sCT**	**CT**	**sCT**	**CT**	**sCT**
Body												
Mean	N/A	-0.4	N/A	-0.1	N/A	-0.2	N/A	-0.1	N/A	-0.3	N/A	-0.1
Max	0.8	-0.7	-1.1	0.5	0.0	-0.1	-0.6	0.0	-0.3	-0.1	-0.5	-0.1
PTV												
Mean	1.0	-0.5	-0.7	0.2	-0.2	-0.2	-0.5	-0.2	-0.5	-0.3	-0.2	0.0
V95%	0.3	-0.1	0.0	0.0	0.0	0.0	0.0	0.0	0.0	0.0	0.0	0.0
D99%	1.4	-0.4	-0.7	0.0	-0.1	0.0	-0.2	0.0	-0.4	-0.3	-0.2	0.0
CTV												
Mean	1.0	-0.5	-0.7	0.2	-0.3	-0.2	-0.6	-0.2	-0.6	-0.3	-0.2	0.0
Min	1.1	-0.7	-0.6	0.0	-0.2	0.0	-0.7	-0.2	-0.7	-0.3	-0.2	0.1
Bladder												
Mean	-1.2	-0.3	1.5	-0.4	1.2	-0.7	0.4	-0.3	1.8	-0.3	-0.6	-0.2
Rectum												
Mean	1.4	-0.6	1.6	-0.2	-0.2	-0.2	0.4	0.0	1.4	-0.1	0.6	-0.1
V90%	9.6	-2.6	0.0	0.5	-1.3	-0.4	-0.2	-0.3	-1.9	-0.7	0.3	-0.6
V75%	4.3	-1.1	1.3	-0.8	0.3	-0.4	1.4	-0.1	0.2	0.0	0.4	-0.2
V65%	2.9	-0.8	3.1	0.0	0.8	-0.4	1.9	-0.1	0.7	0.0	0.2	-0.1
Femoral heads												
Mean	-1.1	-0.3	-0.7	-0.8	0.7	-0.6	-0.6	-0.1	0.5	0.0	-0.1	0.0
Max	3.2	-0.5	-0.7	-1.0	1.3	-0.8	0.1	0.7	-1.5	-0.4	-0.2	0.0

Appendix III - DVH parameters for proton treatment plans.

Proton treatment planning results for each patient case. The result from the DVH comparison between the rCT and the CT and sCT, respectively, is shown in the table below. Results presented in percent.

	Case 1		Case 2		Case 3		Case 4		Case 5		Case 6	
	CT	**sCT**	**CT**	**sCT**	**CT**	**sCT**	**CT**	**sCT**	**CT**	**sCT**	**CT**	**sCT**
Body												
Mean	N/A	0.1	N/A	0.2	N/A	-0.4	N/A	-0.4	N/A	0.2	N/A	0.8
Max	0.0	0.6	-0.1	0.4	0.6	0.7	-0.4	0.8	0.3	0.1	0.6	0.1
PTV												
Mean	-0.3	-0.1	0.0	-0.2	-0.3	-0.1	-0.7	0.0	-0.1	-0.1	-0.2	-0.4
V95%	-1.7	-0.1	-0.1	-0.2	-0.3	-0.1	-1.6	-0.1	-0.3	-0.2	-0.1	-0.1
D99%	-2.8	-0.6	-0.1	-0.7	-0.7	-0.5	-3.9	-0.4	-0.6	-0.6	-0.7	-0.7
CTV												
Mean	-0.1	0.0	0.0	0.0	-0.2	0.0	-0.2	0.0	-0.1	0.0	-0.2	-0.2
Min	-0.6	-0.3	-0.4	-0.4	-0.4	-0.4	-0.7	-0.4	-0.1	0.0	-0.8	-0.7
Bladder												
Mean	15.5	-0.3	-4.0	-0.3	2.5	-0.7	3.5	-0.4	0.5	0.4	0.3	1.0
Rectum												
Mean	-6.3	-0.1	3.3	-1.3	-1.0	-0.2	-5.5	0.3	2.0	0.1	1.1	-0.4
V90%	-7.8	-1.0	4.0	5.3	-3.6	-0.3	-11.7	2.1	2.4	0.5	-1.3	-1.7
V75%	-6.7	-0.2	3.8	-1.3	-2.0	-0.3	-8.3	0.5	1.3	0.2	0.2	-0.4
V65%	-6.7	0.0	4.0	-0.9	-1.4	-0.3	-7.1	0.2	1.7	0.1	0.6	-0.4
Femoral heads												
Mean	10.7	0.0	-1.6	0.0	0.4	0.0	4.6	0.1	-0.8	-0.2	-2.0	-0.7
Max	-0.1	-0.6	-0.2	0.2	0.0	0.1	-0.7	0.8	-1.3	-0.3	-1.5	-0.8

Appendix IV – Fiducial marker identification observer study results.

In the table below the results from the fiducial marker identification study are shown for case 1 and case 2. The observers are named 1-6 and the markers 1-3 as described in section 3.6.2. The numbers in red indicates the marker which was identified wrong, and therefore not included in the standard deviation.

Patient	Marker	Position	1	2	3	4	5	6	Standard deviation [mm]
Patient 1	1	X	36.5	36.7	36.8	36.6	37.0	36.7	0.2
		Y	79.2	79.2	79.3	79.2	79.2	79.5	0.1
		Z	5.1	5.2	6.1	5.8	6.1	6.2	0.5
	2	X	0.4	-3.0	-3.1	-3.1	-2.9	-3.2	1.4
		Y	69.2	69.2	69.2	69.2	6.92	68.0	0.5
		Z	5.1	1.8	2.8	2.0	1.7	2.3	1.3
	3	X	32.2	32.3	32.0	31.6	32.1	32.2	0.3
		Y	69.2	69.2	69.1	69.2	69.2	68.8	0.2
		Z	-1.4	-1.2	-1.0	-1.1	-1.3	-1.1	0.1
Patient 2	1	X	8.1	8.6	8.9	7.9	8.5	8.8	0.4
		Y	-9.5	-7.0	-7.4	-9.5	-7.0	-7.6	1.2
		Z	16.1	17.1	16.4	17.0	16.1	16.7	0.4
	2	X	-14.0	-14.0	-14.2	-14.0	-13.8	-14.3	0.2
		Y	-17.0	-17.0	-16.8	-1.70	-17.0	-17.0	0.1
		Z	9.3	9.3	.93	9.2	9.2	9.1	0.1
	3	X	7.4	7.8	7.1	6.9	1.5	7.4	0.3
		Y	-12.0	-12.0	-12.1	-14.5	3.0	-12.0	1.1
		Z	2.2	2.3	2.4	3.1	23.7	2.4	0.4

Appendix V - Fiducial marker identification observer study results.

In the table below the results from the fiducial marker identification study are shown for case 3 and case 4. The observers are named 1-6 and the markers 1-3 as described in section 3.6.2.

Patient	Marker	Position	1	2	3	4	5	6	Standard deviation [mm]
Patient 3	1	X	25.8	25.8	25.8	26.4	25.8	25.8	0.2
		Y	16.9	16.9	16.9	16.9	16.9	16.9	0.0
		Z	0.0	0.3	0.5	0.4	0.4	0.4	0.2
	2	X	-6.3	-6.0	-6.3	-6.3	-6.3	-6.3	0.1
		Y	6.9	6.9	6.9	6.9	6.9	6.9	0.0
		Z	0.8	0.0	0.4	0.6	0.4	0.4	0.3
	3	X	1.3	1.3	1.6	1.7	1.7	1.6	0.2
		Y	1.9	1.9	2.8	4.4	1.9	3.4	1.0
		Z	-3.2	-2.9	-3.0	-3.6	-2.7	-3.1	0.3
Patient 4	1	X	-1.0	-1.6	-1.8	-1.5	-1.4	-1.1	0.3
		Y	22.6	22.6	21.6	22.6	22.6	22.6	0.4
		Z	55.7	34.9	35.5	35.2	35.0	35.6	8.4
	2	X	-23.3	-23.0	-22.9	-23.2	-23.3	-23.1	0.2
		Y	27.6	27.6	27.3	27.6	27.6	27.1	0.2
		Z	36.6	36.2	36.5	36.5	36.4	36.9	0.2
	3	X	-5.5	-5.9	-6.0	-6.1	-5.9	-6.1	0.2
		Y	17.6	17.6	18.7	17.6	17.6	19.5	0.8
		Z	37.9	38.8	38.4	38.3	37.7	38.2	0.4

Appendix VI – DICE calculation

In the table below the DICE calculation for patient case 1-3 are shown. The calculations are done in 20 slices and the mean value of these presented at the bottom of each row. The DICE value is in percent.

	Case 1		**Case 2**		**Case 3**	
Slice	**sCT**	**CT**	**sCT**	**CT**	**sCT**	**CT**
20	86.9	93.1	84.6	93.3	91.3	92.7
21	86.7	93.4	85.4	94.4	91.0	93.7
22	87.5	92.3	85.6	94.1	90.7	92.8
23	87.1	93.7	85.5	93.2	89.8	91.3
24	86.2	93.4	85.0	93.4	89.5	89.0
25	86.5	93.1	85.6	93.0	89.1	91.3
26	86.3	93.7	86.1	91.3	89.4	89.8
27	85.9	92.4	86.1	91.6	88.6	87.7
28	85.7	92.9	86.0	92.2	87.5	90.2
29	87.2	93.9	85.7	90.5	88.1	88.7
30	86.5	91.8	85.3	89.8	86.4	91.1
31	86.1	93.3	86.2	91.8	83.3	92.3
32	82.7	91.7	85.2	91.4	86.3	92.6
33	81.3	89.3	84.8	92.2	91.1	92.4
34	81.8	89.4	87.1	93.1	89.8	92.9
35	83.0	87.7	86.4	91.1	87.0	90.5
36	82.7	84.4	85.8	90.3	88.1	88.8
37	85.4	91.5	84.7	90.6	86.9	88.0
38	84.4	92.9	82.6	89.9	86.1	88.1
39	84.9	86.3	83.5	90.6	87.9	90.3
40	88.6	93.6	81.8	89.7	87.9	89.6
Mean	**85.4**	**91.6**	**85.2**	**91.8**	**88.4**	**90.7**

Appendix VII – DICE calculation

In the table below the DICE calculation for patient case 4-6 are shown. The calculations are done in 20 slices and the mean value of these presented at the bottom of each row. The DICE value is in percent.

	Case 4		**Case 5**		**Case 6**	
Slice	sCT	CT	sCT	CT	sCT	CT
20	88.6	96.2	89.6	96.0	90.4	94.3
21	88.9	95.2	89.5	94.8	89.8	93.8
22	89.0	96.2	89.9	95.6	89.6	93.6
23	88.5	96.2	89.8	95.4	89.6	93.1
24	88.8	95.4	90.7	95.0	90.0	93.0
25	89.3	95.8	91.3	95.7	90.6	93.9
26	89.7	95.8	91.1	95.8	90.9	94.6
27	89.6	95.4	90.7	95.4	91.1	93.2
28	89.7	93.6	90.7	95.6	90.9	94.3
29	89.2	95.3	90.7	95.4	90.3	94.4
30	89.0	94.8	90.0	94.3	90.2	93.1
31	88.8	93.1	89.6	95.8	90.2	93.7
32	88.3	94.5	88.4	93.7	87.7	95.6
33	87.3	93.1	88.9	93.4	90.3	95.1
34	85.8	92.6	89.9	95.9	92.4	95.0
35	84.6	88.1	89.5	94.6	91.6	96.0
36	84.1	86.8	89.2	93.4	91.1	94.7
37	89.0	94.2	88.8	95.0	89.5	94.4
38	88.4	94.5	88.2	94.4	87.8	95.1
39	88.7	89.6	85.0	92.9	89.5	92.7
40	83.2	86.4	85.1	93.8	89.3	95.0
Mean	**88.0**	**93.5**	**89.4**	**94.8**	**90.1**	**94.2**